



Thermo-elasticity displacement formulation for constrained articulated mechanical systems

Ahmed A. Shabana^a, Mahmoud Elbakly^{a,b}, Moataz Abdalla^a, and Ahmed E. Eldeeb^{a,b}

^aDepartment of Mechanical and Industrial Engineering, University of Illinois at Chicago, Chicago, IL, USA; ^bDepartment of Mechanical Design and Production Engineering, Cairo University, Giza, Egypt

ABSTRACT

This paper proposes an approach for thermal analysis of articulated systems subject to boundary and motion constraints (BMC). The solution framework is designed to capture large temperature fluctuations, significant change in geometry due to reference configuration and deformations, and geometric nonlinearity due to articulated mechanical systems (AMS) large displacements and spinning motion. Thermal-expansion displacements, which do not contribute to rigidbody translations, are determined from thermal stretch of position-gradient vectors using a new sweeping matrix technique designed to eliminate dependence on translational rigid-body modes. A new quadratic thermal-energy kinetic form is defined and used to formulate a dynamic force vector that accounts for thermal transient and inertia effects. Nodal thermal displacements are used in formulating AMS differential/algebraic equations (DAEs), and consequently, thermal stresses due to BMC equations are automatically accounted for based on integration of thermal analysis and Lagrange-D'Alembert principle, which is the foundation of computational multibody system (MBS) algorithms. The approach used in this study for large-displacement constrained and unconstrained thermal expansions is based on multiplicative decomposition of position-gradient matrix, instead of strain additive decomposition, for solution of thermo-elasticity problems. Four configurations are used to define continuum geometry and displacements: straight configuration, reference configuration, thermal-expansion configuration, and current configuration. The proposed approach allows applying thermal loads during constrained large displacements, does not impose restrictions on the choice of thermal coefficients, captures reference-configuration geometry and change in inertia forces due to temperature fluctuations, accounts for thermal displacement in formulating AMS nonlinear constraint equations, and allows for integration with MBS algorithms for the study of a wide range of thermo-elasticity problems.

ARTICLE HISTORY

Received 28 September 2022 Accepted 28 February 2023

KEYWORDS

Displacement thermoelasticity; thermo-elasticity multiplicative decomposition; finite-element thermal analysis; articulated mechanical systems; absolute nodal coordinate formulation

1. Introduction

Change of continuum temperature due to heat energy input produces particle displacements. Heat energy, however, does not produce rigid-body displacements, does not contribute to stress-producing elastic strains (Cook 1981), and leads to thermal expansion, during which part of the thermal energy is converted to kinetic energy. In case of constrained mechanical systems, displacement formulation of the thermal expansion process becomes necessary to formulate correctly kinematic constraint equations imposed on the system motion. Furthermore, definition of thermal-energy forces that produce the motion allows for properly capturing transient effects of the thermo-elasticity problem and eliminates the need for formulating thermal-stress forces as in the case of the conventional FE approach.

1.1. Displacement formulation thermal-energy forces

In the analysis of flexible *articulated mechanical systems* (AMS), algebraic constraint equations that impose motion restrictions are formulated in terms of material-point displacements and/or vectors defined at the material points. In absence of specified-motion trajectories, coordinates of material points are not explicit functions of time, and in this case, global position vector \mathbf{r} of arbitrary point of a system component can be written as $\mathbf{r} = \mathbf{r}(\mathbf{q}(t))$, where \mathbf{q} is the vector of system generalized coordinates and t is time. Because vector \mathbf{r} is not explicit function of time, $\partial \mathbf{r}/\partial t = \mathbf{0}$ and the absolute velocity vector can be written as $\dot{\mathbf{r}} = (\partial \mathbf{r}/\partial \mathbf{q})\dot{\mathbf{q}}$. In the case of the thermo-elasticity, on the other hand, material-point position in the current configuration can be written as $\mathbf{r} = \mathbf{r}_o + \mathbf{u}_s + \mathbf{u}_\Theta$, where $\mathbf{r}_o = \mathbf{X}$ is the position in the reference configuration, \mathbf{u}_s is the displacement that includes rigid-body displacement and stress-producing deformation, and \mathbf{u}_Θ is the *thermal expansion displacement*. Thermal-expansion displacement vector \mathbf{u}_Θ for a given temperature profile is explicit function of time and needs to be defined properly to formulate correctly AMS inertia forces and nonlinear boundary and motion constraints (BMC) that restrict thermal expansion and lead to thermal loads and stresses.

Nonetheless, motion constraints are formulated in terms of the total displacements, which are affected by the heat energy input. Consequently, if the thermal displacement can be determined, the heat-energy input can be used to formulate thermal-energy forces that can be used with other forces to solve for the total displacements. Thermal-energy forces, however, are distinguished from other forces since they produce pure deformation and do not lead to rigid-body displacements. Therefore, thermal-displacement vector \mathbf{u}_{Θ} , used to formulate thermal-energy forces, does not have rigid-body modes and can be expressed as linear combination of deformation modes. Consequently, thermal-energy forces excite only deformation modes.

1.2. Lagrange-D'Alembert principle

Despite the significance of the problem and the wide range of applications, the scientific literature lacks a general approach to study effects of thermal-load variations on AMS dynamics and stability. Properly accounting for the coupling between thermal expansion and nonlinear motion constraints in AMS applications with components that experience finite rotations is one of the main challenges that will be addressed in this study by integrating Lagrange-D'Alembert principle and large-displacement thermo-elasticity analysis. Articulated mechanical systems are subjected to highly nonlinear motion constraints that must be enforced at position, velocity, and acceleration levels during numerical integration of the equations of motion. AMS applications, governed by Lagrange-D'Alembert principle, often operate in high-temperature environment, as in case of piston-crank mechanisms, commonly used in engines. Components of such articulated systems, widely used in practice, undergo large displacements and can operate at high speeds. Furthermore, thermal loads have significant effect on dynamics and precision of soft robots and deployable space structures that may operate in high-temperature environment (Rus and Tolley 2015; Trivedi, Dienno, and Rahn 2008; Wu, Zhao, and Ren 2012). Nonetheless, there are no approaches in the literature for solving AMS thermo-elasticity problems in case of large displacements, significant temperature variations, and presence of joint constraints.

1.3. Thermal stresses due to motion constraints

Two different cases of thermal displacements can be considered: stress-free and stress-producing thermal displacements. In case of unconstrained stress-free thermal displacements, thermal

expansion is assumed uniform such that stretches are not restricted by loads or motion constraints. This case, which does not require thermal-displacement formulation, can be solved by updating the stress-free reference configuration geometry to account for the thermal expansion and properly define the elastic strains. In this case, only thermally stretched gradients are sufficient to determine updated reference configuration. In the second case, thermal displacements occur during system motion and load application. This case requires displacement formulation of the thermo-elasticity problem to account for the transient effects. In case of BMC restrictions, some gradients become dependent variables and must be determined from the independent variables according to Lagrange-D'Alembert principle.

1.4. Thermo-elasticity multiplicative decomposition

Accurate quantification of temperature effect contributes to developing credible virtual models, particularly when such an effect cannot be ignored as evident by large number of investigations in areas of solid and fluid mechanics as well as other areas of science and engineering (Biot 1956; Perelman 1961; Helselhaus, Vogel, and Krain 1992; Chang et al. 1999; API MPMS 2004; Huang and Tan 2004; Yin and Wang 2004; Roe, Haselbacher and Geubelle 2007; Roe et al. 2008; Henshaw and Chand 2009; Dorfman and Renner 2009; Heidarpour and Bradford 2009; Dwaikat and Kodur 2011; Errera and Chemin 2013; Eslami et al. 2013; Ojas and Penelope 2014; Cui, Yu, and Lan 2019; Shen and Hu 2013; Shen et al. 2013, 2020; Abbas, Rui, and Marzocca 2015; Čepon et al. 2017; Li, Wang, Ma, et al. 2019; Seibert and Rice 1973; Shabana 1986). In conventional FE thermo-elasticity approaches, the strain additive decomposition is often used (Cook 1981). This assumption, however, is not applicable to large-displacement thermal analysis of AMS applications. Additionally, multiplicative decomposition of matrix of position-gradient vectors, instead of additive strain decomposition, must be used. Furthermore, reference-configuration geometry needs to be accurately described using geometry concepts that play important role in formulation of continuum governing equations (Goetz 1970; Kreyszig 1991; Piegl and Tiller 1997; Rogers 2001; Farin 2002; Gallier 2011). Geometry change has significant effects on the dynamic behavior (Chen, Zhang, and Li 2019), and consequently this change should be accurately captured. The absolute nodal coordinate formulation (ANCF), used recently in many applications, has the advantage of using position-gradient vectors as nodal coordinates which allow describing conveniently reference and thermal-expansion configurations (Orzechowski 2012; Orzechowski and Fraczek 2012; Khan and Anderson 2013; Laflin et al. 2014; Dmitrochenko and Pogorelov 2003; Yu et al. 2010; Yoo et al. 2004; Takahashi, Shimizu, and Suzuki 2005; Nachbagauer et al. 2011; Nachbagauer 2013, 2014; Fotland, Haskins, and Rølvåg 2019; Hewlett 2019; Hewlett, Arbatani, and Kovecses 2020; Sheng, Zhong, and Wang 2020; Tian et al. 2009; Wang and Wang 2020; Yuan et al. 2020; Zhang, Zhu, and Zhang 2020; Yamano et al. 2020; Htun, Suzuki, and Garcia-Vallejo 2020; Pan and Cao 2020; Gerstmayr and Shabana 2005).

2. Scope and contributions of this investigation

Due to the lack of computational approaches for solving AMS thermo-elasticity problems in case of large displacements, significant temperature variations, and presence of joint constraints, new AMS thermo-elasticity approach is proposed in this study for homogeneous materials and uniform temperature fields. AMS components, subjected to boundary and motion constraints, may undergo arbitrarily large displacements. The proposed solution framework, which integrates Lagrange-D'Alembert principle and large-displacement thermal analysis based on multiplicative decomposition of the position-gradient matrix, allows formulating BMC equations in terms of thermal expansion displacements. The specific objectives and contributions of this study are summarized as follows:

- 1. New formulation and solution procedure, referred to as thermal analysis of articulated systems (TAAS), is developed for AMS thermo-elasticity problems, in which system components subjected to boundary and motion constraints may undergo arbitrarily large displacements and temperature variations. The new approach lies at the intersection of thermal science, computational design, and computational geometry. The resulting TAAS solution framework is based on integrating Lagrange-D'Alembert principle and large-displacement multiplicative-decomposition thermal analysis (MDTA).
- 2. The paper demonstrates the need for determining thermal-displacement vector \mathbf{u}_{Θ} due to thermal expansion to formulate properly BMC conditions and equations of motion of AMS applications. It is shown that definition of thermo-elasticity problem at strain levels is not sufficient, and definition of thermal-displacement vector \mathbf{u}_{Θ} in terms of stretches of position gradients is necessary in order to formulate properly AMS thermo-elasticity problem.
- 3. A new procedure is developed to determine thermal-displacement \mathbf{u}_{Θ} using general continuum mechanics description. Since thermal expansion and position gradients do not contribute to rigid-body translations, a procedure similar to the *sweeping matrix technique* used in vibration theory is developed and used to eliminate dependence of assumed thermal-displacement field on rigid-body motion. To this end, new orthogonality conditions are introduced and used to eliminate singularities of new coefficient-matrices used in the development of the new approach.
- 4. A new quadratic form of the thermal energy, referred to as thermal-energy kinetic form E_{tk} , is developed using time derivatives of thermal-displacement vector \mathbf{u}_{Θ} . Thermal energy is expressed as quadratic form in the velocities, leading to the definition of a new dynamic force vector that accounts for the transient effect of the thermal process. The thermal-energy kinetic form is used to define new thermal-energy forces that enter into the formulation of the continuum equations of motion.
- 5. The new approach is integrated with new continuum-mechanics description based on *multiplicative decomposition* of the position-gradient matrix to allow for arbitrary temperature variations and large-displacement thermal analysis of *MBS applications*. Analysis of such systems requires treatment of nonlinear algebraic motion constraint equations. To this end, four configurations are employed: *straight configuration*, *reference configuration*, *thermal-expansion configuration*, and *current configuration*. Use of these configurations allows capturing temperature fluctuations, complex reference-configuration geometry, and space-dependent thermal-expansion and material coefficients. The multiplicative-decomposition approach is more suitable for use in emerging fields such as soft robots subjected to large deformations and high temperatures (Rus and Tolley 2015, Huang, Zou, and Gu 2021).
- 6. New computer algorithm for solving general AMS differential/algebraic equations (DAEs) is developed and used to demonstrate effect of BMC restrictions on AMS geometry and dynamics. Coupled nonlinear motion and BMC differential/algebraic equations are formulated to properly account for the thermal displacements and effects of BMC restrictions on constrained expansion and inertia forces. Dependent gradients are identified and written in terms of independent system coordinates to solve correctly the constrained thermo-elasticity problems.
- 7. Fundamental differences between proposed solution framework and conventional FE thermal-analysis approaches are highlighted throughout this study. Use of *absolute nodal coordinate formulation* (ANCF) position-gradient vectors as nodal coordinates allows describing conveniently reference and thermal-expansion configurations by directly using nodal coordinates (Pappalardo, Yu, et al. 2016; Pappalardo, Wallin, et al. 2016). Furthermore, fully parameterized ANCF elements capture Poisson effect, required for accurate modeling of cross-section deformations during process of thermal expansion. Examples are used in this study to demonstrate coupling between AMS large displacements, BMC restrictions, and thermal expansion.

Crucial for developing the TAAS approach introduced in this study is using ANCF position gradients as FE nodal coordinates. ANCF position gradients allow defining thermal-displacement vector using deformation modes as the basis and allow capturing complex reference-configuration geometry (Omar et al. 2004).

3. Constrained thermal expansion

In case of AMS thermal analysis, BMC restrictions can significantly alter strain field and introduce high-frequency inertia forces and high thermal stresses (Pournaghshbanda 2019). To capture properly constrained thermal expansions, thermal displacements must be defined using thermal stretch of position gradients.

3.1. Problem definition

Thermal displacements enter into definition of nonlinear BMC algebraic equations, which define mechanical joints and specified trajectories. BMC equations impose restrictions on thermal expansions since some gradients or strains become dependent variables and are determined using independent coordinates. This AMS thermal expansion problem can be addressed in the framework of Lagrange-D'Alembert principle, required for proper treatment of constrained dynamics problems.

Solution framework introduced in this paper is based on applying BMC conditions to AMS coordinates, which may include reference coordinates for rigid bodies, modal coordinates for small-deformation floating frame of reference (FFR) bodies, and position-gradients for soft ANCF bodies. Lagrange-D'Alembert principle is used to express dependent variables in terms of independent variables or degrees of freedom using velocity transformation. Large-deformation thermal expansion of soft materials is accounted for using the matrix of position gradients. Using this geometric approach, time and space variations of temperature profiles and spatial and temporal dependence of thermal and material coefficients can be accounted for. Nonlinear BMC equations, which influence the geometry, can be enforced at position, velocity, and acceleration levels to avoid violation of Lagrange-D'Alembert principle and ensure using proper procedure for time integration of equations of motion.

3.2. Thermal effect on kinematics

Position vector of continuum material points can be written as $\mathbf{r}(\mathbf{X},t) = \mathbf{X} + \mathbf{u}(\mathbf{X},t)$, where \mathbf{X} is the vector of reference-configuration coordinates, \mathbf{u} is the displacement vector, and t is time. In case of thermal expansion, the position vector, as previously discussed, can be written as $\mathbf{r} =$ $X + u_{\Theta} + u_{s}$, where displacement vector u is written as sum of two displacement vectors: \mathbf{u}_{Θ} resulting from thermal expansion and u_s which includes stress producing deformation and rigidbody displacements. Thermal stresses can be attributed to BMC conditions that change definition of elastic forces and can introduce high frequencies that directly influence the accelerations. In presence of kinematic constraints, all forces including inertia forces must be properly projected on space of degrees of freedom, and regardless of magnitude of \mathbf{u}_{Θ} , BMC conditions can significantly change stresses and inertia forces. Thermal displacement vector \mathbf{u}_{Θ} can be determined from thermally expanded gradients using the equation $d\mathbf{u}_{\Theta} = \mathbf{J}_{d\Theta} d\mathbf{X}$, where $\mathbf{J}_{d\Theta}$ is the matrix of displacement-gradient vectors due to thermal expansion.

3.3. AMS topology

AMS applications contain bodies with different degrees of flexibility. Bulky bodies are often modeled as rigid bodies whose motion is described using reference coordinates \mathbf{q}_r , small-deformation flexible bodies modeled using approximation functions or low-frequency modal coordinates \mathbf{q}_f , and soft and fluid bodies whose motion is described using ANCF coordinates \mathbf{e} . Use of these three different types of coordinates allows solving accurately AMS applications that may include large number of components with varied degree of flexibility. Therefore, general AMS algorithms are designed to have coordinate vector $\mathbf{q} = \begin{bmatrix} \mathbf{q}_r^T & \mathbf{q}_f^T & \mathbf{e}^T \end{bmatrix}^T$. In MBS dynamics, joint constraints and specified motion trajectories are described using nonlinear algebraic equations that can be written as $\mathbf{C}(\mathbf{q},t) = \mathbf{C}(\mathbf{q}_r,\mathbf{q}_f,\mathbf{e},t) = \mathbf{0}$. MBS algorithms are designed to solve DAE system according to Lagrange-D'Alembert principle.

Effect of BMC restrictions on accuracy of thermal-expansion solution can be explained using the simple example shown in Fig. 1, which depicts a beam subjected to thermal load. For this system, two clamped-joint types can be applied at first beam end. In first type, referred to as *partially clamped*, position coordinates and rotations at the fixed end are constrained, with no constraints imposed on strains, and therefore, thermal expansion is homogeneous throughout the beam. In second constraint type, referred to as *fully clamped*, additional boundary constraints are imposed on position gradients, resulting in the tapered shape shown in the figure. This simple example demonstrates effect of boundary constraints on geometry and displacement of material points and need for proper treatment of the algebraic equations during thermal expansion process.

3.4. Stretch of gradient vectors

In case of fully parameterized ANCF elements, position gradients at a node are defined by $\mathbf{r}_{x_k} = \partial \mathbf{r}/\partial x_k$, k=1,2,3, where $\mathbf{x} = \begin{bmatrix} x_1 & x_2 & x_3 \end{bmatrix}^T = \begin{bmatrix} x & y & z \end{bmatrix}^T$ is vector of element spatial coordinates. For such fully parameterized ANCF elements, for example, coordinates at a node are defined by node position vector \mathbf{r} and three gradient vectors $\mathbf{r}_{x_k} = \partial \mathbf{r}/\partial x_k$, k=1,2,3. Stretch of gradient vector due to thermal expansion is $d_{ok}(1+\alpha_{\Theta k}\Delta\Theta)$, k=1,2,3, where d_{ok} is the magnitude of the gradient vector before thermal expansion, $\alpha_{\Theta k}$ is coefficient of thermal expansion, and $\Delta\Theta$ is variation in temperature. In case of unconstrained thermal expansion of homogeneous and isotropic materials, all gradient at all material points stretch by $d_{ok}\alpha_{\Theta k}\Delta\Theta$, k=1,2,3. This is not, however, the case of constrained thermal expansion as demonstrated by the simple beam example of Fig. 1

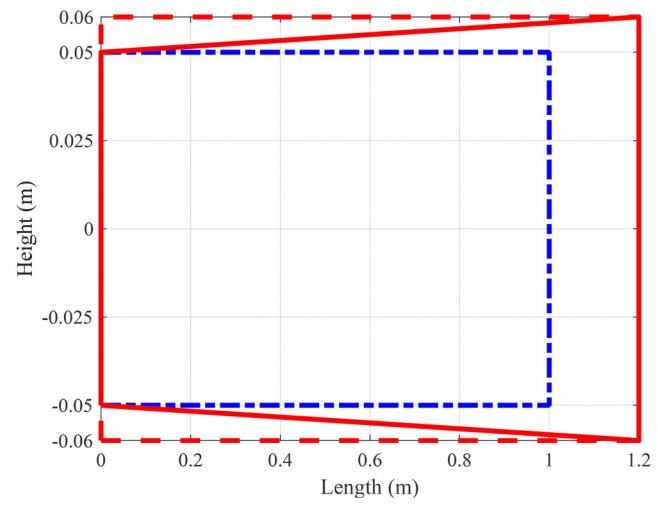


Figure 1. Geometry for different end conditions (— — Initial configuration, — Fully clamped under thermal load, —— Partially clamped under thermal load).

in which fully clamped joint leads to tapered geometry. Some gradients, not necessarily all, can be subjected to BMC restrictions due to enforcing constraints $C(\mathbf{q},t) = C(\mathbf{q}_r,\mathbf{q}_f,\mathbf{e},t) = \mathbf{0}$. That is, stretch of a gradient coordinate can be restricted if such a coordinate is not a degree of freedom. The planar example of Fig. 1 has simple gradient boundary constraints at the fixed end. These constraints imply that gradient vectors remain orthogonal unit vectors, and consequently, the cross section at the fixed end does not stretch since position and rotation constraints only do not restrict cross-section stretch. According to Lagrange-D'Alembert principle, system velocity vector $\dot{\mathbf{q}}$ which includes position-gradient coordinates can be written in terms of independent velocities $\dot{\mathbf{q}}_i$ as $\dot{\mathbf{q}} = \mathbf{B}_{di}\dot{\mathbf{q}}_{i}$, where \mathbf{B}_{di} is velocity transformation defined using nonlinear BMC algebraic equations. It follows that $\ddot{\mathbf{q}} = \mathbf{B}_{di}\ddot{\mathbf{q}}_i + \gamma_{di}$, where γ_{di} is the vector that absorbs terms which are not linear in accelerations. Using this Lagrange-D'Alembert procedure and using iterative Newton-Raphson algorithm at every time step to determine dependent coordinates from constraint equations $C(q,t) = C(q_r,q_f,e,t) = 0$ ensures that all BMC algebraic equations are satisfied at the position level. BMC restrictions on thermal stretch can be properly accounted for at all solution steps (position, velocity, and acceleration). This procedure for treatment of algebraic equations demonstrates that thermal expansion of redundant gradients should be distinguished from thermal expansion associated with gradients identified as independent coordinates; that is, dependent-gradient stretch is determined from independent gradients using BMC algebraic equations, which are nonlinear functions of AMS coordinates.

4. Mechanism of thermal expansion

In the formulation used in this investigation, it is assumed that the reference configuration before displacement is defined by the coordinate vector $\mathbf{X} = \begin{bmatrix} X_1 & X_2 & X_3 \end{bmatrix}^T$. Therefore, the displacement change due to thermal load can be written as

$$d\mathbf{u}_{\Theta} = \mathbf{J}_{d\Theta} d\mathbf{X} \tag{1}$$

where $J_{d\Theta}=\partial u_{\Theta}/\partial X$ is matrix of thermal-expansion displacement-gradient vectors. Referenceconfiguration geometry is defined by the constant position-gradient matrix $\mathbf{J}_o = \partial \mathbf{X}/\partial \mathbf{x}$, where $\mathbf{x} = \begin{bmatrix} x_1 & x_2 & x_3 \end{bmatrix}^T$ is FE spatial coordinates in the straight configurations. Using the equation $d\mathbf{X} = \begin{bmatrix} x_1 & x_2 & x_3 \end{bmatrix}^T$ $J_o dx$, one can also write $d\mathbf{u}_{\Theta} = (J_{d\Theta}J_o)dx$. For homogeneous materials and constant temperature field, the equation $d\mathbf{u}_{\Theta} = \mathbf{J}_{d\Theta} d\mathbf{X}$ leads to

$$\mathbf{u}_{\Theta}(\mathbf{x}) - \mathbf{u}_{\Theta}(\mathbf{x}_o) = \mathbf{J}_{d\Theta}(\mathbf{X} - \mathbf{X}_o) \tag{2}$$

In this equation, \mathbf{x}_0 and $\mathbf{X}_0 = \mathbf{X}(\mathbf{x}_0)$ define reference points in the straight and reference configurations, respectively. If the coordinate system is located at \mathbf{x}_o , one can assume $\mathbf{x}_o = \mathbf{0}$.

Definition of the matrix $J_{d\Theta}$ can be obtained by writing $d\mathbf{r} = d\mathbf{X} + d\mathbf{u}_S + d\mathbf{u}_{\Theta}$. It follows from this equation that $d\mathbf{r} = [\mathbf{I} + (\partial \mathbf{u}_s/\partial \mathbf{X}) + (\partial \mathbf{u}_\Theta/\partial \mathbf{X})]d\mathbf{X}$. Assuming volumetric thermal change, the matrix $\mathbf{J}_{d\Theta} = \partial \mathbf{u}_{\Theta}/\partial \mathbf{X}$, which represents thermal stretches in directions of coordinate lines \mathbf{X} , can be defined as $\mathbf{J}_{d\Theta} = \partial \mathbf{u}_{\Theta}/\partial \mathbf{X} = \Delta \Theta \left[\alpha_{\Theta 1} \hat{\mathbf{a}}_1 \ \alpha_{\Theta 2} \hat{\mathbf{a}}_2 \ \alpha_{\Theta 3} \hat{\mathbf{a}}_3 \right]$, where $\hat{\mathbf{a}}_1, \hat{\mathbf{a}}_2$, and $\hat{\mathbf{a}}_3$ are three unit vectors along the tangents to the coordinate lines $\mathbf{X} = \begin{bmatrix} X_1 & X_2 & X_3 \end{bmatrix}^T$, where $\alpha_{\Theta k}$, k = 1, 2, 3, are coefficients of thermal expansion and $\Delta\Theta$ is the change in temperature.

Using the definition of ANCF displacement field $\mathbf{r} = \mathbf{S}(\mathbf{x})\mathbf{e}(t)$, where \mathbf{r} is the position vector, S is the element shape function matrix, and e is the vector of nodal coordinates; one can write (Li, Wang, Ma, et al. 2019, Nachbagauer et al. 2011; Olshevskiy, Dmitrochenko, and Kim 2014; Shabana 2018)

$$\begin{array}{ll} \mathbf{u}_{\Theta}(\mathbf{x}) = \mathbf{S}(\mathbf{x})\mathbf{e}_{d\Theta}, & \mathbf{u}_{\Theta}(\mathbf{x}_{o}) = \mathbf{S}(\mathbf{x}_{o})\mathbf{e}_{d\Theta}, \\ \mathbf{X}(\mathbf{x}) = \mathbf{S}(\mathbf{x})\mathbf{e}_{o}, & \mathbf{X}(\mathbf{x}_{o}) = \mathbf{S}(\mathbf{x}_{o})\mathbf{e}_{o} \end{array}$$
 (3)

where \mathbf{e}_o is vector of element nodal coordinates in reference configuration, and $\mathbf{e}_{d\Theta}$ is the vector of nodal displacements due to thermal expansion. Substituting the preceding equations into Eq. (2), one can write for arbitrary ANCF element

$$\mathbf{S}_{rd}\mathbf{e}_{d\Theta} = \mathbf{J}_{d\Theta}\mathbf{S}_{rd}\mathbf{e}_{o} \tag{4}$$

In this equation, $\mathbf{S}_{rd} = \mathbf{S}(\mathbf{x}) - \mathbf{S}(\mathbf{x}_o)$ with subscript rd referring to rotation and deformation displacements, as will be discussed. Pre-multiplying the preceding equation by $\rho \mathbf{S}_{rd}^T$, where ρ is element mass density, and integrating over the volume V, one obtains

$$\bar{\mathbf{M}}_{rd}\mathbf{e}_{d\Theta} = \bar{\mathbf{M}}_{1}\mathbf{e}_{o} \tag{5}$$

where $\bar{\mathbf{M}}_{rd} = \int_{V} \rho \mathbf{S}_{rd}^{T} \mathbf{S}_{rd} dV$, $\bar{\mathbf{M}}_{1} = \int_{V} \rho \mathbf{S}_{rd}^{T} \mathbf{J}_{d\Theta} \mathbf{S}_{rd} dV$. Matrix $\bar{\mathbf{M}}_{rd}$, given in the Appendix for planar shear deformable beam element, is symmetric, while matrix $\bar{\mathbf{M}}_{1}$ is block symmetric.

An infinitesimal volume has twelve modes of displacements: three translations, three rotations, and six deformation modes. Nine of these displacement modes are represented by the matrix of position vector gradients; these are three rotations and six deformation modes; with the deformation modes describing three stretch modes and three shear modes (Spencer 1980; Ogden 1984; Bonet and Wood 1997; Bower 2009; Shabana 2018). Therefore, displacements resulting from only stretch of gradient vectors do not contribute to rigid-body translational displacements. Consequently, equation $\mathbf{u}_{\Theta}(\mathbf{x}) - \mathbf{u}_{\Theta}(\mathbf{x}_{o}) = \mathbf{J}_{d\Theta}(\mathbf{X} - \mathbf{X}_{o})$ leads to displacement $\mathbf{u}_{\Theta}(\mathbf{x})$ that does not include rigid-body translations. As will be demonstrated in a later section, if A_r is a rigidbody translational mode, matrix S_{rd} obtained using ANCF finite elements must satisfy the identity $\mathbf{S}_{rd}\mathbf{A}_r = \mathbf{0}$. It will be also shown if $\mathbf{M} = \int_V \rho \mathbf{S}^T \mathbf{S} dV$ is ANCF mass matrix and \mathbf{A}_{r_i} and \mathbf{A}_{r_i} are two rigid-body translational modes, then $\mathbf{A}_{r_i}^T \mathbf{M} \mathbf{A}_{r_i} = 0$ if $i \neq j$ and $\mathbf{A}_{r_i}^T \mathbf{M} \mathbf{A}_{r_i} \neq 0$ if i = j. These identities will be used to define the conditions on thermal-expansion displacements using a concept that resembles the concept of the sweeping matrices used in vibration theory to eliminate dependence of initial guess of higher-frequency modes on lower-frequency modes (Weaver, Timoshenko, and Young 1990; Thomson 1993; Shabana 2019). This translational rigid-body mode elimination process is necessary since thermal expansion does not contribute to rigid-body translations. Elimination of such translational rigid-body modes is also necessary to avoid singular coefficient matrices.

5. Solution for mesh thermal displacements

Determining nodal thermal displacements of FE mesh allows developing *thermal-energy kinetic* form E_{tk} , used in this study to determine *thermal-energy forces* that produce the motion. These forces exist only when second time derivative of temperature is different from zero.

5.1. Element and mesh equations

For an element j of an FE mesh that consists of n_e elements, Eq. (5) can be written as

$$\bar{\mathbf{M}}_{rd}^{j} \mathbf{e}_{d\Theta}^{j} = \bar{\mathbf{M}}_{1}^{j} \mathbf{e}_{o}^{j} \tag{6}$$

This equation can be assembled for all elements of the FE mesh using element Boolean matrix \mathbf{B}^{j} and standard FE assembly procedure to obtain

$$\mathbf{M}_{rd}\mathbf{e}_{d\Theta} = \mathbf{M}_1\mathbf{e}_o \tag{7}$$

where $\mathbf{e}_{d\Theta}$ and \mathbf{e}_o are, respectively, mesh vectors of thermal-displacements and coordinates in the reference configuration, $\mathbf{M}_{rd} = \sum_{j=1}^{n_e} \mathbf{B}^{j^T} \bar{\mathbf{M}}_{rd}^j \mathbf{B}^j$ and $\mathbf{M}_1 = \sum_{j=1}^{n_e} \mathbf{B}^{j^T} \bar{\mathbf{M}}_1^j \mathbf{B}^j$. The preceding equation can also be written as $\mathbf{M}_{rd} \mathbf{e}_{d\Theta} = \mathbf{b}_o$, where $\mathbf{b}_o = \mathbf{M}_1 \mathbf{e}_o$. Because position- and displacement-

gradient vectors do not contribute to rigid-body translation and matrix \mathbf{M}_{rd} is square and symmetric matrix with dimension n_{Θ} where n_{Θ} is dimension of vector $\mathbf{e}_{d\Theta}$; matrix \mathbf{M}_{rd} has rank deficiency equal to number of translational rigid-body modes. Therefore, solution of mesh equation $\mathbf{M}_{rd}\mathbf{e}_{d\Theta}=\mathbf{M}_1\mathbf{e}_o$ to determine $\mathbf{e}_{d\Theta}$ requires eliminating dependence on translational rigidbody modes using a concept that resembles sweeping matrix technique used in matrix iteration method of vibration theory (Weaver et al. 1990; Thomson 1993; Shabana 2019).

5.2. Elimination of translational rigid-body modes

When using ANCF finite elements, vector of nodal coordinates can be written as $\mathbf{e} = \mathbf{e}_o + \mathbf{e}_d$, where \mathbf{e}_o is vector of coordinates in initial reference configuration and \mathbf{e}_d is vector of displacement coordinates. Equation $\mathbf{e} = \mathbf{e}_o + \mathbf{e}_d$ implies that gradient vectors can be added despite the fact that finite rotations are not commutative and cannot be treated as vectors. Therefore, translational rigid-body displacement mode k can always be written in spatial analysis as

$$\mathbf{A}_{r_k} = \left[\mathbf{a}_{r_k}^T \mathbf{0}^T \mathbf{0}^T \mathbf{0}^T \mathbf{a}_{r_k}^T \mathbf{0}^T \mathbf{0}^T \mathbf{0}^T \mathbf{0}^T \cdots \mathbf{a}_{r_k}^T \mathbf{0}^T \mathbf{0}^T \mathbf{0}^T \right]^T$$
(8)

where in this equation $\mathbf{0} = \begin{bmatrix} 0 & 0 & 0 \end{bmatrix}^T$ are associated with displacement gradients at given node, and $\mathbf{a}_{r_1} = \mathbf{i} = \begin{bmatrix} 1 & 0 & 0 \end{bmatrix}^T$ for translation in X_1 direction, $\mathbf{a}_{r_2} = \mathbf{j} = \begin{bmatrix} 0 & 1 & 0 \end{bmatrix}^T$ for translation in X_2 direction, and $\mathbf{a}_{r_3} = \mathbf{k} = \begin{bmatrix} 0 & 0 & 1 \end{bmatrix}^T$ for translation in X_3 direction. When ANCF elements are used, translational rigid-body modes are orthogonal with respect to the ANCF mass matrix. That is, if M is the mesh mass matrix, one has

$$\mathbf{A}_{r_k}^T \mathbf{M} \mathbf{A}_{r_l} = 0 \text{ if } k \neq l
\mathbf{A}_{r_k}^T \mathbf{M} \mathbf{A}_{r_l} \neq 0 \text{ if } k = l$$
(9)

Knowing the form of translational rigid-body modes, one can eliminate dependence of solution $\mathbf{e}_{d\Theta}$ of equation $\mathbf{M}_{rd}\mathbf{e}_{d\Theta}=\mathbf{M}_1\mathbf{e}_o$ on rigid-body translation and solve the singularity problem of matrix \mathbf{M}_{rd} by imposing the following constraint conditions, which ensure that thermal expansion does not contribute to continuum rigid-body translations:

$$\mathbf{A}_{n}^{T}\mathbf{M}\mathbf{e}_{d\Theta} = 0, \quad k = 1, 2, 3 \tag{10}$$

where k refers to translational rigid-body modes in X_k direction. The three preceding mesh algebraic constraint equations can be used to write three nodal displacements, considered as dependent displacements, in terms of the remaining displacements, considered as independent.

Therefore, vector of displacements $\mathbf{e}_{d\Theta}$ can be partitioned as $\mathbf{e}_{d\Theta} = \left[\left(\mathbf{e}_{d\Theta} \right)_d^T \left(\mathbf{e}_{d\Theta} \right)_i^T \right]^T$ where subscripts d and i refer, respectively, to three translational dependent coordinates and (n-3)independent coordinates. Therefore, one can write $\mathbf{e}_{d\Theta} = \mathbf{H}_{di}(\mathbf{e}_{d\Theta})_i$, where \mathbf{H}_{di} is a matrix that allows writing mesh coordinates in terms of the independent coordinates based on constraint equations $\mathbf{A}_{r_k}^T \mathbf{M} \mathbf{e}_{d\Theta} = 0$, k = 1, 2, 3. Substituting transformation $\mathbf{e}_{d\Theta} = \mathbf{H}_{di}(\mathbf{e}_{d\Theta})_i$ into matrix equation $\mathbf{M}_{rd}\mathbf{e}_{d\Theta} = \mathbf{b}_o$ and pre-multiplying by \mathbf{H}_{di}^T , one obtains

$$\left(\mathbf{H}_{di}^{T}\mathbf{M}_{rd}\mathbf{H}_{di}\right)\left(\mathbf{e}_{d\Theta}\right)_{i} = \mathbf{H}_{di}^{T}\mathbf{b}_{o} \tag{11}$$

Matrix $\mathbf{M}_H = \mathbf{H}_{dl}^{\mathsf{T}} \mathbf{M}_{rd} \mathbf{H}_{dl}$ is symmetric and has dimension (n-3). The preceding equation, which ensures that thermal expansion does not contribute to rigid-body translations, can be solved to determine vector $(\mathbf{e}_{d\Theta})_i$. Mesh nodal displacement $\mathbf{e}_{d\Theta}$ can be determined using equation $\mathbf{e}_{d\Theta}$ $\mathbf{H}_{di}(\mathbf{e}_{d\Theta})_i$. The form of the matrix \mathbf{M}_H in the case one ANCF fully parameterized planar beam element is presented in the Appendix of this paper.

5.3. Positive definiteness of M_H

It can be shown that the matrix \mathbf{M}_H , which has dimension (n-3), is always positive-definite matrix guaranteeing solution of equation $(\mathbf{H}_{di}^T\mathbf{M}_{rd}\mathbf{H}_{di})(\mathbf{e}_{d\Theta})_i = \mathbf{H}_{di}^T\mathbf{b}_o$. This is clear from the definition of matrix $\bar{\mathbf{M}}_{rd}$ at element level, which is defined as $\bar{\mathbf{M}}_{rd} = \int_V \rho \mathbf{S}_{rd}^T \mathbf{S}_{rd} dV$. The example of the planar ANCF beam element considered in the Appendix demonstrates this fact.

6. An alternate approach

An alternate and simpler approach for computer implementation to obtain thermal displacements can be developed using inverse of ANCF constant mass matrix. Equation $\mathbf{u}_{\Theta}(\mathbf{x}) - \mathbf{u}_{\Theta}(\mathbf{x}_{o}) = \mathbf{J}_{d\Theta}(\mathbf{X} - \mathbf{X}_{o})$ leads to

$$(\mathbf{S}(\mathbf{x}) - \mathbf{S}(\mathbf{x}_o))\mathbf{e}_{d\theta} = \mathbf{J}_{d\Theta}(\mathbf{S}(\mathbf{x}) - \mathbf{S}(\mathbf{x}_o))\mathbf{e}_o$$
(12)

Multiplying both sides of this equation by $\rho S^T dV$ and integrating over the volume, one obtains

$$\left(\int_{V} \rho \mathbf{S}^{T}(\mathbf{x}) \mathbf{S}(\mathbf{x}) dV - \left(\int_{V} \rho \mathbf{S}^{T}(\mathbf{x}) dV\right) \mathbf{S}(\mathbf{x}_{o})\right) \mathbf{e}_{d\theta}
= \left(\int_{V} \rho \mathbf{S}^{T}(\mathbf{x}) \mathbf{J}_{d\Theta} (\mathbf{S}(\mathbf{x}) - \mathbf{S}(\mathbf{x}_{o})) dV\right) \mathbf{e}_{o}$$
(13)

In this equation, $\int_V \rho \mathbf{S}^T(\mathbf{x}) \mathbf{S}(\mathbf{x}) dV = \mathbf{M}$ is the symmetric and constant ANCF mass matrix, and $\int_V \rho \mathbf{S}(\mathbf{x}) dV = \bar{\mathbf{S}}$ is a constant matrix; in case of planar ANCF shear deformable beam element as shown in the Appendix, this matrix is $\bar{\mathbf{S}} = \int_V \rho \mathbf{S} \, dV = (m/2) \big[\mathbf{I} \, (l/6) \mathbf{I} \, \mathbf{0} \, \mathbf{I} \, -(l/6) \mathbf{I} \, \mathbf{0} \big]$. Therefore, the preceding equation upon pre-multiplying by \mathbf{M}^{-1} leads to

$$\mathbf{I}_{u}\mathbf{e}_{d\theta} = \mathbf{M}^{-1} \left(\int_{V} \rho \mathbf{S}^{T}(\mathbf{x}) \mathbf{J}_{d\Theta} \left(\mathbf{S}(\mathbf{x}) - \mathbf{S}(\mathbf{x}_{o}) \right) dV \right) \mathbf{e}_{o}$$
 (14)

where $\mathbf{I}_u = \mathbf{I} - \mathbf{M}^{-1} \bar{\mathbf{S}}^T \mathbf{S}(\mathbf{x}_o)$. Singularity of this matrix can be eliminated by eliminating rigid-body modes using the equation $\mathbf{e}_{d\Theta} = \mathbf{H}_{di}(\mathbf{e}_{d\Theta})_i$ previously presented in this paper. Pre-multiplying $\mathbf{I}_u \mathbf{e}_{d\Theta} = \mathbf{M}^{-1}(\int_V \rho \mathbf{S}^T(\mathbf{x}) \mathbf{J}_{d\Theta}(\mathbf{S}(\mathbf{x}) - \mathbf{S}(\mathbf{x}_o)) dV) \mathbf{e}_o$ by \mathbf{H}_{di}^T and using transformation $\mathbf{e}_{d\Theta} = \mathbf{H}_{di}(\mathbf{e}_{d\Theta})_i$, one obtains

$$\left(\mathbf{H}_{di}^{T}\mathbf{I}_{u}\mathbf{H}_{di}\right)\left(\mathbf{e}_{d\theta}\right)_{i} = \mathbf{H}_{di}^{T}\mathbf{M}^{-1}\left(\int_{V} \rho \mathbf{S}^{T}(\mathbf{x})\mathbf{J}_{d\Theta}\left(\mathbf{S}(\mathbf{x}) - \mathbf{S}(\mathbf{x}_{o})\right)dV\right)\mathbf{e}_{o}$$
(15)

In this equation, matrix $\mathbf{H}_{di}^T \mathbf{I}_u \mathbf{H}_{di}$ is nonsingular, and therefore, the preceding equation can be solved for independent thermal displacements. Using the equation $d\mathbf{u}_{\Theta} = \mathbf{J}_{d\Theta} \mathbf{J}_o d\mathbf{x}$ and assuming that element coordinate system is attached to first node, one can write the preceding equation as

$$\left(\mathbf{H}_{di}^{T}\mathbf{I}_{u}\mathbf{H}_{di}\right)\left(\mathbf{e}_{d\Theta}\right)_{i} = \mathbf{H}_{di}^{T}\mathbf{M}^{-1}\left(\int_{V} \rho \mathbf{S}^{T}(\mathbf{x})(\mathbf{J}_{d\Theta}\mathbf{J}_{o})\mathbf{x}dV\right)$$
(16)

where $\mathbf{x} = \begin{bmatrix} x_1 & x_2 & x_3 \end{bmatrix}^T = \begin{bmatrix} x & y & z \end{bmatrix}^T$ One can show that the right side of this equation can be written in terms of the integrals $\int_V \rho x \mathbf{S}^T(\mathbf{x}) dV$, $\int_V \rho y \mathbf{S}^T(\mathbf{x}) dV$, and $\int_V \rho z \mathbf{S}^T(\mathbf{x}) dV$.

7. Thermal-energy kinetic form

In the absence of BMC restrictions, thermal expansion does not contribute to the stress-producing elastic strains (Cook 1981). That is, in case of non-zero second time derivative of the

temperature, the heat energy converted to kinetic energy leads to dynamic forces that must be defined and entered to the equations of motion in case of known temperature profiles. The heat energy considered in this section does not include energy dissipated to the environment, and consequently, heat dissipation to the surroundings and cooling effects are not considered. The inertia force of an infinitesimal volume ρdV due to thermal expansion can be written as $(\rho dV)\ddot{\mathbf{u}}_{\Theta}$, where $\ddot{\mathbf{u}}_{\Theta}$ is the acceleration vector due to the thermal expansion. The virtual work of this inertia force can be written as $(\rho dV)\ddot{\mathbf{u}}_{\Theta} \cdot \delta \mathbf{r} = (\rho dV)\ddot{\mathbf{u}}_{\Theta} \cdot (\partial \mathbf{r}/\partial \mathbf{e})\delta \mathbf{e}$, where \mathbf{e} is the vector of ANCF coordinates. Therefore, for the FE mesh, one can write

$$\int_{V} \rho \ddot{\mathbf{u}}_{\Theta} \cdot \delta \mathbf{r} dV = \left[\int_{V} \rho \ddot{\mathbf{u}}_{\Theta} \cdot (\partial \mathbf{r} / \partial \mathbf{e}) \, dV \right] \delta \mathbf{e} \tag{17}$$

Because $\partial \mathbf{r}/\partial \mathbf{e} = \partial \dot{\mathbf{r}}/\partial \dot{\mathbf{e}}$ and considering the change due to thermal expansion only in a more general case in which the temperature is not prescribed, that is, $\partial \mathbf{r}/\partial \mathbf{e} = \partial \mathbf{u}_{\Theta}/\partial \mathbf{e}$ and $\partial \dot{\mathbf{r}}/\partial \dot{\mathbf{e}} = \partial \mathbf{u}_{\Theta}/\partial \mathbf{e}$ $\partial \dot{\mathbf{u}}_{\Theta}/\partial \dot{\mathbf{e}}$, the term on the right side of the preceding equation can be written as

$$\left[\int_{V} \rho \ddot{\mathbf{u}}_{\Theta} \cdot (\partial \mathbf{u}_{\Theta} / \partial \mathbf{e}) \, dV \right] \delta \mathbf{e}
= \left(d \left[\int_{V} \rho \dot{\mathbf{u}}_{\Theta} \cdot (\partial \dot{\mathbf{u}}_{\Theta} / \partial \dot{\mathbf{e}}) \, dV \right] / dt - \left[\int_{V} \rho \dot{\mathbf{u}}_{\Theta} \cdot (\partial \dot{\mathbf{u}}_{\Theta} / \partial \mathbf{e}) \, dV \right] \right) \delta \mathbf{e}$$
(18)

Introducing quadratic velocity thermal-energy kinetic function $E_{tk} = (\int_V \rho \dot{\mathbf{u}}_{\Theta} \cdot \dot{\mathbf{u}}_{\Theta} dV)/2$, the preceding equation can be written as

$$\left[\int_{V} \rho \ddot{\mathbf{u}}_{\Theta} \cdot (\partial \mathbf{u}_{\Theta} / \partial \mathbf{e}) \, dV\right] \delta \mathbf{e} = \left(d[\partial E_{tk} / \partial \dot{\mathbf{e}}] / dt - [\partial E_{tk} / \partial \mathbf{e}]\right) \delta \mathbf{e} \tag{19}$$

The thermal-energy kinetic function can be written for the FE mesh as

$$E_{tk} = \left(\int_{V} \rho \dot{\mathbf{u}}_{\Theta} \cdot \dot{\mathbf{u}}_{\Theta} dV \right) / 2 = \left(\dot{\mathbf{e}}_{d\Theta}^{T} \mathbf{M} \dot{\mathbf{e}}_{d\Theta} \right) / 2 \tag{20}$$

where M is the FE mass matrix. Since, for ANCF elements, $\mathbf{e} = \mathbf{e}_o + \mathbf{e}_d = \mathbf{e}_o + \mathbf{e}_{ds} + \mathbf{e}_{d\Theta}$ and since in case of ANCF finite elements E_{tk} depends only on $\dot{\mathbf{e}}_{d\Theta}$, $\partial E_{tk}/\partial \dot{\mathbf{e}} = \partial E_{tk}/\partial \dot{\mathbf{e}}_{d\Theta}$ and $\partial E_{tk}/\partial \mathbf{e} = \partial E_{tk}/\partial \mathbf{e}_{d\Theta}$, where \mathbf{e}_{ds} is the vector of nodal displacements used to define \mathbf{u}_s . In this case, one can define the thermal-energy dynamic force vector

$$\mathbf{Q}_{tk} = \left(d[\partial E_{tk}/\partial \dot{\mathbf{e}}_{d\Theta}]/dt - [\partial E_{tk}/\partial \mathbf{e}_{d\Theta}]\right)^{T}$$
(21)

Because E_{tk} is quadratic in the velocities and **M** is constant, one has

$$\mathbf{Q}_{tk} = \left(d[\partial E_{tk}/\partial \dot{\mathbf{e}}_{d\Theta}]/dt\right)^{T} = \mathbf{M}\ddot{\mathbf{e}}_{d\Theta}$$
(22)

For given temperature profile, this thermal dynamic force vector can be computed and added to the generalized force vector of the system equations of motion. Because thermal expansion does not contribute to the stress-producing elastic strains (Cook 1981), $\mathbf{e}_{d\Theta}$ does not lead to elastic stresses. In case of large-displacement analysis, multiplicative decomposition is used based on the four configurations discussed in the following section.

In this study, the second-order differential equations of motion associated with the independent variables are transformed to first-order differential equations using the state vector $\mathbf{y} =$ $\begin{bmatrix} \mathbf{e}_{di}^T \ \dot{\mathbf{e}}_{di}^T \end{bmatrix}^T$, where subscript *i* refers to independent coordinates. The state equations to be numerically integrated are defined as $\dot{\mathbf{y}} = \mathbf{f}(\mathbf{y}, t) = \begin{bmatrix} \dot{\mathbf{e}}_{di}^T \ \ddot{\mathbf{e}}_{di}^T \end{bmatrix}^T$. In case of linearly varying temperature, $\ddot{\mathbf{e}}_{d\Theta} = \mathbf{0}$ while $\dot{\mathbf{e}}_{d\Theta}$ may be different from zero. Since $\mathbf{y} = \begin{bmatrix} \mathbf{e}_{di}^T \ \dot{\mathbf{e}}_{di}^T \end{bmatrix}^T$ is the output of the numerical integration and cannot be changed while the function $\dot{\mathbf{y}} = \mathbf{f}(\mathbf{y},t) = \begin{bmatrix} \dot{\mathbf{e}}_{di}^T \ddot{\mathbf{e}}_{di}^T \end{bmatrix}^T$ is being evaluated, $\dot{\mathbf{e}}_{di}$ should be updated by the time derivatives of the thermal displacement only in the vector $\dot{\mathbf{y}} = \mathbf{f}(\mathbf{y},t) = \begin{bmatrix} \dot{\mathbf{e}}_{di}^T \ddot{\mathbf{e}}_{di}^T \end{bmatrix}^T$ before returning to the numerical integrator. That is, the case of linearly varying temperature can be treated in a manner similar to the case of linearly varying displacement of a body in case of zero resultant force.

8. Thermal-expansion configuration

In case of large strains, use of assumptions of strain additive decomposition often adopted in FE literature for small-deformation thermal analysis is not recommended (Zienkiewicz 1977; Zienkiewicz and Taylor 2000). In strain additive decompositions, based on super-position principle, displacement gradients (not position gradients) are used to define thermal expansion. This simplified approach, which has been used with conventional FE displacement fields, does not allow for properly capturing complex reference-configuration geometries and large displacements. In the conventional thermal-analysis, normal strains are written as linear functions of gradients of displacement vector $\mathbf{u} = \begin{bmatrix} u_1 & u_2 & u_3 \end{bmatrix}^T$ as $\varepsilon_{ii} = \partial u_i / \partial x_i$, i = 1, 2, 3. Such linearization neglects geometric nonlinearities and is not applicable to large-displacement analysis. In the strain additive decomposition, total strain $\varepsilon = (\mathbf{J}^T \mathbf{J} - \mathbf{I})/2$, assumed known from solving system equations, is sum of elastic strain ε_e and stress-free thermal strain ε_{Θ} , that is, $\varepsilon = \varepsilon_e + \varepsilon_{\Theta}$, written in Voigt vector form as $(\mathbf{\epsilon})_{v} = \begin{bmatrix} \varepsilon_{11} & \varepsilon_{22} & \varepsilon_{33} & \varepsilon_{12} & \varepsilon_{13} & \varepsilon_{23} \end{bmatrix}^{T}$, where ε_{ii} , i = 1, 2, 3, and ε_{ij} , $i \neq j$, i, j = 1, 2, 3, are, respectively, normal and shear strains. Stress-free thermal strain is written as $(\varepsilon_{\Theta})_{\nu}$ $\begin{bmatrix} \alpha_{\Theta 1} \Delta \Theta & \alpha_{\Theta 2} \Delta \Theta & \alpha_{\Theta 3} \Delta \Theta & 0 & 0 & 0 \end{bmatrix}^T$, where $\alpha_{\Theta i}$, i = 1, 2, 3, are coefficients of thermal expansion, and $\Delta\Theta$ is temperature change (Cook, 1981; Liu and Lu 2007; Logan 2017). Therefore, the stress-producing elastic strain is defined as $(\varepsilon_e)_{\nu} = (\varepsilon)_{\nu} - (\varepsilon_{\Theta})_{\nu}$. This definition of the elastic strains commonly used in the FE literature implies that the thermal expansion does not contribute to the stress forces.

8.1. Multiplicative decomposition

In analysis of large-displacements, *multiplicative decomposition* of matrix of position-gradient vectors is used (Eckart 1948; Kroner 1959; Sedov 1966; Stojanovic, Djuric, and Vujosevic 1964; Stojanovic 1969; Stojanovic, Vujosevic, and Blagojevic 1970; Miehe 1995; Imam and Johnson 1998; Lubarda 2004; Longère et al. 2005; Darijani and Kargarnovin 2010; Darijani 2012; Darijani and Naghdabadi 2013; Sadik and Yavari 2017; Sauer, Ghaffari, and Gupta 2019; Vujosevic and Lubarda 2002; Joulin, Xiang, and Latham 2020). As shown in Fig. 2, continuum kinematics in thermal analysis can be described using four different configurations: *straight configuration* defined by coordinates $\mathbf{x} = \begin{bmatrix} x_1 & x_2 & x_3 \end{bmatrix}^T$, reference configuration defined by $\mathbf{X} = \begin{bmatrix} X_1 & X_2 & X_3 \end{bmatrix}^T$, thermal expansion configuration defined by $\mathbf{X}_{\Theta} = \begin{bmatrix} X_{\Theta 1} & X_{\Theta 2} & X_{\Theta 3} \end{bmatrix}^T$, and current configuration defined by $\mathbf{r} = \begin{bmatrix} r_1 & r_2 & r_3 \end{bmatrix}^T$. These four configurations, based on definition of position gradients as tangent to coordinate lines and need to be distinguished from displacement gradients, are discussed in detail in the literature (Shabana and Zhang 2021; Shabana 2015).

Using these four configurations allows for defining two different types of reference configurations; one stress-free reference configuration before displacements and the other is thermal-expansion reference configuration. These two reference configurations are distinguished by the parameters used. Vector \mathbf{r} in the current configuration can, therefore, have the following two different representations: $\mathbf{r} = \mathbf{X} + \mathbf{u}_{\Theta} + \mathbf{u}_s = \mathbf{X}_{\Theta} + \mathbf{u}_s$. Use of these two reference configurations is discussed below.

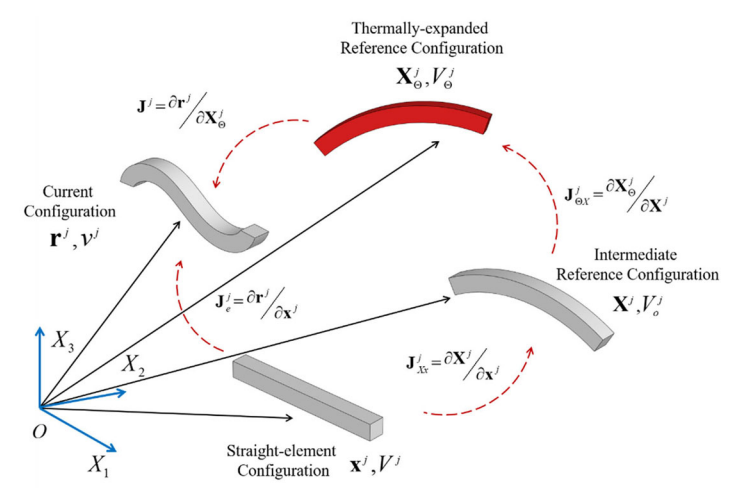


Figure 2. Continuum configurations.

8.2. Stress-free reference configuration

In case of using stress-free reference configuration before displacements, parameter vector X is used, and current configuration is defined by equation $\mathbf{r} = \mathbf{X} + \mathbf{u}_{\Theta} + \mathbf{u}_{s}$. In this case,

$$d\mathbf{r} = \mathbf{J}d\mathbf{X} = (\mathbf{I} + (\partial \mathbf{u}_{\Theta}/\partial \mathbf{X}) + (\partial \mathbf{u}_{s}/\partial \mathbf{X}))d\mathbf{X}$$

$$= (\mathbf{I} + [(\partial \mathbf{u}_{\Theta}/\partial \mathbf{x}) + (\partial \mathbf{u}_{s}/\partial \mathbf{x})]\mathbf{J}_{o}^{-1})d\mathbf{X}$$
(23)

In this equation,

$$\mathbf{J} = \mathbf{I} + (\partial \mathbf{u}_{\Theta} / \partial \mathbf{X}) + (\partial \mathbf{u}_{S} / \partial \mathbf{X}) = \mathbf{I} + [\mathbf{J}_{d\Theta_{\ell}} + \mathbf{J}_{dS_{\ell}}] \mathbf{J}_{0}^{-1}$$
(24)

where $\mathbf{J}_o = \partial \mathbf{X}/\partial \mathbf{x}$, and

$$\mathbf{J}_{d\Theta e} = (\partial \mathbf{u}_{\Theta} / \partial \mathbf{x}) = \partial (\mathbf{S}(\mathbf{x}) \mathbf{e}_{d\Theta}) / \partial \mathbf{x}
\mathbf{J}_{dse} = (\partial \mathbf{u}_{s} / \partial \mathbf{x}) = \partial (\mathbf{S}(\mathbf{x}) \mathbf{e}_{ds}) / \partial \mathbf{x}$$
(25)

It is clear from these definitions that the position-gradient vectors, unlike finite rotations, are commutative and can be added and subtracted. Since $\mathbf{e}_{d\Theta}$, determined from known temperature profile, does not contribute to elastic forces, one can define matrix of position-gradient vectors $\bar{\mathbf{J}}_s$ and elastic strain ε_e that enter into formulation of the stress forces as

$$\bar{\mathbf{J}}_{s} = \mathbf{I} + (\partial \mathbf{u}_{s}/\partial \mathbf{X}) = \mathbf{I} + \mathbf{J}_{dse} \mathbf{J}_{o}^{-1}
\mathbf{\varepsilon}_{e} = (1/2)(\bar{\mathbf{J}}_{s}^{T} \bar{\mathbf{J}}_{s} - \mathbf{I})$$
(26)

Using vector of elastic strains ε_e ensures, in the absence of constraints, that thermal expansion vector $\mathbf{e}_{d\Theta}$ does not contribute to stresses, as it is assumed in the FE literature.

8.3. Updated thermal reference configuration

Alternatively, one can write $\mathbf{r} = \mathbf{X}_{\Theta} + \mathbf{u}_s$. In this case, $\mathbf{X}_{\Theta} = \mathbf{S}(\mathbf{x})(\mathbf{e}_o + \mathbf{e}_{d\Theta})$ is used as reference configuration, and one can write

$$d\mathbf{r} = (\partial \mathbf{r}/\partial \mathbf{X}_{\Theta})d\mathbf{X}_{\Theta} = \mathbf{J}_{\Theta}d\mathbf{X}_{\Theta} = (\mathbf{J}_{e}\mathbf{J}_{\Theta x}^{-1})d\mathbf{X}_{\Theta}$$
 (27)

In this equation, $J_{\Theta} = \partial \mathbf{r}/\partial \mathbf{X}_{\Theta}$, $J_{e} = \partial \mathbf{r}/\partial \mathbf{x}$ and $J_{\Theta x} = \partial \mathbf{X}_{\Theta}/\partial \mathbf{x}$. In this alternate approach, elastic Green-Lagrange strain tensor is defined as $\mathbf{\epsilon}_e = (1/2)(\mathbf{J}_{\Theta}^T\mathbf{J}_{\Theta} - \mathbf{I})$. This definition of elastic strains ensures that reference configuration geometry and thermal expansion do not contribute to stress forces

ANCF finite elements have been also used in the thermo-elasticity analysis in different applications (Shen and Hu 2013; Shen et al. 2013; Abbas, Rui, and Marzocca 2015; Čepon et al. 2017; Li, Wang, Ma, et al. 2019). However, these investigations are not based on the multiplicative-decomposition and thermal-displacement approach adopted in this study.

9. AMS thermo-elastic and inertia forces

Constrained thermal expansion influences both inertia and elastic forces. BMC restrictions can produce significant compressive elastic forces that influences frequency contents in system accelerations, which in turn influence inertia forces (Seibert and Rice 1973; Manolis and Beskos 1980). If the temperature profile is known, the heat energy input to the system is known and thermal-displacement profile can be determined and used to evaluate the thermal-energy force vector \mathbf{Q}_{tk} , which can be added to the equations of motion as generalized thermal forces. In AMS applications, in which identification of the system degrees of freedom plays a central role in the solution algorithm, thermal displacements cannot be separated from the total displacements during the DAE numerical solution, despite the fact that the thermal displacements can be determined using the known temperature profile. For this reason, part of the analysis presented in Sec. 9.1 is of theoretical nature.

9.1. Thermal-inertia forces

Thermal-expansion vector \mathbf{u}_{Θ} enters into definition of the global position vector $\mathbf{r} = \mathbf{X} + \mathbf{u}_s + \mathbf{u}_{\Theta} = \mathbf{S}(\mathbf{x})(\mathbf{e}_o + \mathbf{e}_{ds} + \mathbf{e}_{d\Theta})$, where \mathbf{u}_s is displacement that includes rigid-body displacement and stress-producing deformations, \mathbf{e}_{ds} is vector of nodal displacements associated with \mathbf{u}_s , and $\mathbf{e}_{d\Theta}$ is thermal-expansion nodal displacement vector determined using the procedure previously discussed. Because, for given temperature profile, $\delta \mathbf{u}_{\Theta} = \mathbf{0}$, virtual displacement and acceleration vectors can be written, respectively, as $\delta \mathbf{r} = \delta \mathbf{u}_s = \mathbf{S}(\mathbf{x})\delta \mathbf{e}_{ds}$ and $\ddot{\mathbf{r}} = \ddot{\mathbf{u}}_s + \ddot{\mathbf{u}}_{\Theta} = \mathbf{S}(\mathbf{x})(\ddot{\mathbf{e}}_{ds} + \ddot{\mathbf{e}}_{d\Theta})$. Virtual work of continuum inertia forces can then be written as $\delta W_i = \int_V \rho \ddot{\mathbf{r}}^T \delta \mathbf{r} dV = (\ddot{\mathbf{e}}_{ds} + \ddot{\mathbf{e}}_{d\Theta})^T \left[\int_V \rho \mathbf{S}^T \mathbf{S} dV\right] \delta \mathbf{e}_{ds}$, which can be written as $\delta W_i = (\mathbf{M}\ddot{\mathbf{e}}_{ds} - \mathbf{Q}_{i\Theta})^T \delta \mathbf{e}_{ds}$, where $\mathbf{M} = \int_V \rho \mathbf{S}^T \mathbf{S} dV$ is constant and symmetric mass matrix, and $\mathbf{Q}_{i\Theta} = -\mathbf{M}\ddot{\mathbf{e}}_{d\Theta}$ is the contribution of thermal expansion to the vector of inertia forces. In case of slow unconstrained thermal-expansion process, vector $\mathbf{Q}_{i\Theta}$ may not be significant. However, BMC restrictions in case of constrained thermal expansion can lead to high-frequency accelerations that influence magnitude of inertia force vector $\mathbf{Q}_{i\Theta}$ because oscillations of the dependent gradient vectors along which the thermal expansion is defined will depend on the continuum oscillations.

In the numerical implementation, it is not recommended to formulate the system equations of motion in terms of \mathbf{e}_{ds} because BMC restrictions are applied to the vector of total displacements \mathbf{e}_d and not to \mathbf{e}_{ds} . Using \mathbf{e}_d instead of \mathbf{e}_{ds} in formulating the equations of motion significantly reduces the efforts required to implement thermo-elasticity formulation discussed in this investigation in general-purpose MBS algorithms since other previously developed force elements and joint constraints do not need to be modified. For this reason, the total displacement vector is used to formulate the equations of motion and thermal-energy force vector \mathbf{Q}_{tk} is added to the right-hand side of the equations of motion as generalized thermal forces. Furthermore, in the case of coupled thermo-mechanical problems, the temperature profile may not be specified since the temperature is determined from the solution of the heat equation which is solved simultaneously with the system equations of motion.



9.2. Thermo-elastic forces

Thermal-analysis approach used in this study is applicable to both unconstrained and constrained thermal expansions. The difference between the two cases is BMC constraints used to determine displacements as result of thermal-load application. Using multiplicative decomposition with ANCF elements, which impose no restrictions on amount of FE deformation or rotation, general non-incremental thermal-analysis formulations can be developed to account accurately for reference-configuration geometry. General form of Green-Lagrange strain tensor, written in terms of position-gradient vectors, allows defining elastic strains using inverse of matrix of position-gradient vectors in the reference configuration.

In case of complex geometry, position-gradient vectors in the reference configuration may not be unit vectors. In this more general case, dimensionless thermal expansions $\alpha_{\Theta k}\Delta\Theta$, k=1,2,3,can be related directly to stretch of corresponding dimensionless non-unit position-gradient vectors \mathbf{r}_{X_k} , k = 1, 2, 3, as

$$(\mathbf{r}_{X_k})_{o+\Theta} = d_{ok}(\hat{\mathbf{r}}_{X_k})_o + (\alpha_{\Theta k} \Delta \Theta) d_{ok}(\hat{\mathbf{r}}_{X_k})_o = d_{ok}(1 + \alpha_{\Theta k} \Delta \Theta)(\hat{\mathbf{r}}_{X_k})_o, \quad k = 1, 2, 3$$
 (28)

where d_{ok} is the length of gradient vector \mathbf{r}_{X_k} before thermal-load application, and $\hat{\mathbf{r}}_{X_k}$ is unit vector along position-gradient vector \mathbf{r}_{X_k} . Using the preceding equation, stretch of position-gradient vectors, which accounts for combined effects of reference-configuration geometry and thermal expansion, can be determined and used to define elastic Green-Lagrange strain tensor as $\mathbf{\epsilon}_e = (\mathbf{J}^T \mathbf{J} - \mathbf{I})/2 = (\mathbf{J}_{o+\Theta}^{-1^T} (\mathbf{J}_e^T \mathbf{J}_e) \mathbf{J}_{o+\Theta}^{-1} - \mathbf{J}_e^T \mathbf{J}_e)$ I)/2, where in this definition $\mathbf{J} = \partial \mathbf{r}/\partial \mathbf{X}_{\Theta} = \mathbf{J}_{e}\mathbf{J}_{o+\Theta}^{-1}$, $\mathbf{J}_{e} = \partial \mathbf{r}/\partial \mathbf{x}$, $\mathbf{J}_{o+\Theta} = \mathbf{J}_{\Theta X}\mathbf{J}_{o}$, and $\mathbf{J}_{\Theta X} = \partial \mathbf{X}_{\Theta}/\partial \mathbf{X}$. The fact that $J_{o+\Theta} = J_{\Theta X}J_o = J_{\Theta X}$ demonstrates equivalence of strain tensor ε_e obtained in this section and definition $\mathbf{\epsilon}_{\epsilon} = (1/2)(\mathbf{J}_{\Theta}^{T}\mathbf{J}_{\Theta} - \mathbf{I})$ obtained in the preceding section. Using this strain tensor and stress-strain relationship defined by material constitutive model, virtual work of stress forces can be written as $\delta W_s = -\int_V \mathbf{\sigma} : \delta \mathbf{\epsilon}_e dV = \mathbf{Q}_s^T \delta \mathbf{q}_e$, where $\mathbf{\sigma}$ is the second Piola-Kirchhoff stress tensor, V is volume in the reference configuration, \mathbf{Q}_s is vector of stress forces, and \mathbf{q}_e is vector of elastic coordinates that can be FFR modal coordinates \mathbf{q}_f or ANCF absolute coordinates \mathbf{e} . Total vector of system coordinates can be writ-

ten as $\mathbf{q} = \begin{bmatrix} \mathbf{q}_r^T \ \mathbf{q}_e^T \end{bmatrix}^T$, where \mathbf{q}_r is vector of reference coordinates. Using this partitioning, virtual work of stress forces can be written as

$$\delta W_s = -\int_V \mathbf{\sigma} : \delta \mathbf{\epsilon}_e dV = \mathbf{Q}_s^T \delta \mathbf{q}_e = \begin{bmatrix} \mathbf{0} \ \mathbf{Q}_s^T \end{bmatrix} \begin{bmatrix} \delta \mathbf{q}_r \\ \delta \mathbf{q}_e \end{bmatrix} = \mathbf{Q}_{sr}^T \delta \mathbf{q}$$
(29)

In this equation, $\mathbf{Q}_{sr}^T = \begin{bmatrix} \mathbf{0} & \mathbf{Q}_s^T \end{bmatrix}$. In case of AMS analysis, virtual change in vector of system coordinates can be written in terms of virtual change of independent coordinates as $\delta \mathbf{q} = \mathbf{B}_{di} \delta \mathbf{q}_i$, where \mathbf{B}_{di} is velocity transformation that accounts for BMC algebraic equations. It follows that thermo-elastic stress forces associated with the independent coordinates in case of constrained thermal expansion can be written as $\mathbf{Q}_{si} = \mathbf{B}_{di}^T \mathbf{Q}_{sr}$. This equation explains the role of the nonlinear BMC algebraic equations in the definition of AMS thermo-elastic forces.

10. ANCF finite elements

ANCF displacement field of an element can be written as $\mathbf{r}(\mathbf{x},t) = \mathbf{S}(\mathbf{x})\mathbf{e}(t)$, where the shape function matrix **S** can always be written in terms of n_{sf} shape functions s_k , $k = 1, 2, ..., n_{sf}$ as

$$\mathbf{S} = \left[s_1 \mathbf{I} \ s_2 \mathbf{I} \cdots s_{n_s f} \mathbf{I} \right] \tag{30}$$

For most ANCF elements, $S(\mathbf{x}_o)$ can be written as $S(\mathbf{x}_o) = [\mathbf{I} \ \mathbf{0} \ \cdots \ \mathbf{0}]$. It follows that

$$\mathbf{S}_{rd} = \mathbf{S}(\mathbf{x}) - \mathbf{S}(\mathbf{x}_o) = \left[(s_1 - 1)\mathbf{I} \ s_2\mathbf{I} \cdots s_{n_{sf}}\mathbf{I} \right]$$
(31)

This equation implies that the element matrix $\bar{\mathbf{M}}_{rd} = \int_V \rho \mathbf{S}_{rd}^T \mathbf{S}_{rd} dV$ differs from the element mass matrix $\mathbf{M} = \int_V \rho \mathbf{S}^T \mathbf{S} dV$ only in the first n_{rg} rows and first n_{rg} column, where n_{rg} is the number of translational rigid-body modes. Furthermore, since $\mathbf{S}_{rd} = \mathbf{S}(\mathbf{x}) - \mathbf{S}(\mathbf{x}_o)$ does not account for rigid-body translations and describes relative motion between material points, one has $\mathbf{S}_{rd}(\mathbf{x})\mathbf{A}_{r_k} = \mathbf{0}$, k = 1, 2, 3, for a rigid-body mode \mathbf{A}_{r_k} of the finite element as defined previously in this paper. It is also to be noted that $\mathbf{S}(\mathbf{x})\mathbf{A}_{r_k} = \mathbf{a}_{r_k}$, k = 1, 2, 3, where \mathbf{a}_{r_k} was previously defined. Therefore, equation $\mathbf{S}_{rd} = \mathbf{S}(\mathbf{x}) - \mathbf{S}(\mathbf{x}_o)$ shows that $\mathbf{S}(\mathbf{x}_o)\mathbf{A}_{r_k} = \mathbf{a}_{r_k}$, k = 1, 2, 3. Nonetheless, Eq. (31) shows that $\mathbf{S}_{rd}(\mathbf{x})\mathbf{e}$ and $\mathbf{S}(\mathbf{x})\mathbf{e}$ lead to same definition of gradients since $\partial \mathbf{S}_{rd}/\partial x_k = \partial \mathbf{S}/\partial x_k$, k = 1, 2, 3. Consequently, the constraint conditions $\mathbf{A}_{r_k}^T \mathbf{M} \mathbf{e}_{d\Theta} = 0$, k = 1, 2, 3, used to ensure that thermal expansion does not contribute to rigid-body translation and eliminate singularity of the element matrix $\bar{\mathbf{M}}_{rd}$, have no effect on the gradient vectors. This is attributed to the fact that gradient vectors describe different displacement modes, mainly rotations and deformations. This important result demonstrates that the process of eliminating rigid-body modes has no influence on thermal stretch of gradient vectors used to define nodal displacements.

Considering the alternate approach for obtaining thermal displacements using the inverse of the ANCF constant mass matrix, matrix $\bar{\mathbf{S}} = \int_V \rho \mathbf{S}(\mathbf{x}) dV$ and mass matrix $\mathbf{M} = \int_V \rho \mathbf{S}^T \mathbf{S} dV$ are defined explicitly for the planar fully parameterized ANCF beam element in the Appendix. Matrix $\mathbf{I}_u = \mathbf{I} - \mathbf{M}^{-1} \bar{\mathbf{S}}^T \mathbf{S}(\mathbf{x}_o)$ that appears in the equation $\mathbf{I}_u \mathbf{e}_{d\theta} = \mathbf{M}^{-1} (\int_V \rho \mathbf{S}^T(\mathbf{x}) \mathbf{J}_{d\Theta}(\mathbf{S}(\mathbf{x}) - \mathbf{S}(\mathbf{x}_o)) dV) \mathbf{e}_o$ can then be written as

$$\mathbf{I}_{u} = \begin{bmatrix} \mathbf{0} & \mathbf{0} & \mathbf{0} & \mathbf{0} & \mathbf{0} & \mathbf{0} \\ \mathbf{0} & \mathbf{I} & \mathbf{0} & \mathbf{0} & \mathbf{0} \\ \mathbf{0} & \mathbf{0} & \mathbf{I} & \mathbf{0} & \mathbf{0} \\ -\mathbf{I} & \mathbf{0} & \mathbf{0} & \mathbf{I} & \mathbf{0} & \mathbf{0} \\ \mathbf{0} & \mathbf{0} & \mathbf{0} & \mathbf{0} & \mathbf{I} & \mathbf{0} \\ \mathbf{0} & \mathbf{0} & \mathbf{0} & \mathbf{0} & \mathbf{0} & \mathbf{I} \end{bmatrix}$$

$$(32)$$

Given the rigid-body modes $\begin{bmatrix} \mathbf{A}_{r1} & \mathbf{A}_{r2} \end{bmatrix} = \begin{bmatrix} \mathbf{I} & \mathbf{0} & \mathbf{0} & \mathbf{I} & \mathbf{0} & \mathbf{0} \end{bmatrix}^T$ in the case of one element, matrix \mathbf{H}_{di} used in transformation $\mathbf{e}_{d\Theta} = \mathbf{H}_{di}(\mathbf{e}_{d\Theta})_i$ previously presented in this paper can be defined for the planar shear-deformable ANCF beam element. Using this matrix, one can show that coefficient matrix $\mathbf{H}_{di}^T \mathbf{I}_u \mathbf{H}_{di}$ which appears in the equation $(\mathbf{H}_{di}^T \mathbf{I}_u \mathbf{H}_{di})(\mathbf{e}_{d\theta})_i = \mathbf{H}_{di}^T \mathbf{M}^{-1}(\int_V \rho \mathbf{S}^T(\mathbf{x}) \mathbf{I}_{d\Theta}(\mathbf{S}(\mathbf{x}) - \mathbf{S}(\mathbf{x}_o))dV)\mathbf{e}_o$ and its inverse can be written, respectively, as

$$\mathbf{H}_{di}^{T}\mathbf{I}_{u}\mathbf{H}_{di} = \begin{bmatrix} \mathbf{I} & \mathbf{0} & \mathbf{0} & \mathbf{0} & \mathbf{0} \\ \mathbf{0} & \mathbf{I} & \mathbf{0} & \mathbf{0} & \mathbf{0} \\ (l/6)\mathbf{I} & \mathbf{0} & 2\mathbf{I} & -(l/6)\mathbf{I} & \mathbf{0} \\ \mathbf{0} & \mathbf{0} & \mathbf{0} & \mathbf{I} & \mathbf{0} \\ \mathbf{0} & \mathbf{0} & \mathbf{0} & \mathbf{0} & \mathbf{I} \end{bmatrix}$$
(33)

and



It can also be shown for the planar ANCF shear-deformable beam element that

$$\mathbf{M}^{-1}\bar{\mathbf{S}}^{T} = \begin{bmatrix} \mathbf{I} \\ \mathbf{0} \\ \mathbf{0} \\ \mathbf{I} \\ \mathbf{0} \\ \mathbf{0} \end{bmatrix}, \quad \mathbf{M}^{-1}\bar{\mathbf{S}}^{T}\mathbf{S}(\mathbf{x}_{o}) = \begin{bmatrix} \mathbf{I} & \mathbf{0} & \mathbf{0} & \mathbf{0} & \mathbf{0} & \mathbf{0} \\ \mathbf{0} & \mathbf{0} & \mathbf{0} & \mathbf{0} & \mathbf{0} & \mathbf{0} \\ \mathbf{0} & \mathbf{0} & \mathbf{0} & \mathbf{0} & \mathbf{0} & \mathbf{0} \\ \mathbf{I} & \mathbf{0} & \mathbf{0} & \mathbf{0} & \mathbf{0} & \mathbf{0} \\ \mathbf{0} & \mathbf{0} & \mathbf{0} & \mathbf{0} & \mathbf{0} & \mathbf{0} \\ \mathbf{0} & \mathbf{0} & \mathbf{0} & \mathbf{0} & \mathbf{0} & \mathbf{0} \end{bmatrix}$$
(35)

In case of planar shear-deformable ANCF element, one can also show that

$$\mathbf{I}_{x} = \int_{V} \rho x \mathbf{S} dV = (ml/10) [(3/2)\mathbf{I} (l/3)\mathbf{I} \mathbf{0} (7/2)\mathbf{I} - (l/2)\mathbf{I} \mathbf{0}]
\mathbf{I}_{y} = \int_{V} \rho y \mathbf{S} dV = (mh^{2}/24) [\mathbf{0} \mathbf{0} \mathbf{I} \mathbf{0} \mathbf{0} \mathbf{I}]$$
(36)

Using results of this integration, it can be shown that

$$\begin{pmatrix} \mathbf{H}_{di}^{T} \mathbf{I}_{u} \mathbf{H}_{di} \end{pmatrix}^{-1} \mathbf{H}_{di}^{T} \mathbf{M}^{-1} \mathbf{I}_{x}^{T} = \begin{bmatrix} \mathbf{I} & \mathbf{0} & (l/2)\mathbf{I} & \mathbf{I} & \mathbf{0} \end{bmatrix}^{T} \\
(\mathbf{H}_{di}^{T} \mathbf{I}_{u} \mathbf{H}_{di})^{-1} \mathbf{H}_{di}^{T} \mathbf{M}^{-1} \mathbf{I}_{y}^{T} = \begin{bmatrix} \mathbf{0} & \mathbf{I} & \mathbf{0} & \mathbf{0} & \mathbf{I} \end{bmatrix}^{T}
\end{pmatrix}$$
(37)

These equations lead to

$$\mathbf{H}_{di} \left(\mathbf{H}_{di}^{T} \mathbf{I}_{u} \mathbf{H}_{di} \right)^{-1} \mathbf{H}_{di}^{T} \mathbf{M}^{-1} \mathbf{I}_{x}^{T} = \begin{bmatrix} -(l/2) \mathbf{I} & \mathbf{I} & \mathbf{0} & (l/2) \mathbf{I} & \mathbf{0} \end{bmatrix}^{T} \\
\mathbf{H}_{di} \left(\mathbf{H}_{di}^{T} \mathbf{I}_{u} \mathbf{H}_{di} \right)^{-1} \mathbf{H}_{di}^{T} \mathbf{M}^{-1} \mathbf{I}_{y}^{T} = \begin{bmatrix} \mathbf{0} & \mathbf{I} & \mathbf{0} & \mathbf{0} & \mathbf{I} \end{bmatrix}^{T}$$
(38)

These equations demonstrate that the two ends of the elements move in opposite directions when rigid-body translations are eliminated. Position-gradient stretches lead only to deformation modes, and therefore, thermal expansion does not lead to element rotations. More details on the matrices of the planar beam are presented in the Appendix.

11. Numerical results

To demonstrate use of the proposed ANCF approach for the thermal expansion, numerical examples are considered in this section. The first example is unconstrained ANCF beam element subjected to thermal load, while the second example is a slider crank mechanism with thermal load applied to the flexible connecting rod. This slider crank mechanism example demonstrates the application of the ANCF thermal-analysis approach to articulated mechanical systems (AMS). The fully parameterized planar ANCF shear deformable beam elements are used in the FE discretization in the two examples. The general continuum mechanics (GCM) approach with planestress assumption is used in the formulation of the elastic forces. The results are obtained using general-purpose MBS software SIGMA/SAMS (Systematic Integration of Geometric Modeling and Analysis for the Simulation of Articulated Mechanical Systems).

11.1. Unconstrained beam

The first example is a free-free beam described using one ANCF element subjected to different thermal loads as shown in Fig. 3. The beam has length l=1 m, cross-section area A= $0.1 \times 0.1 \,\mathrm{m}^2$, mass density $\rho = 7200 \,\mathrm{kg/m}^3$, Young's modulus $E = 7 \times 10^8 \,\mathrm{Pa}$, and Poisson ratio $\nu=0.3$. The material is assumed isotropic with linear coefficient of thermal expansion $\alpha=$ $0.0001 (1/^{\circ}C)$ (Engineering ToolBox 2003). Figure 4 shows the three different temperature profiles used in this example as function of time. These profiles, which have maximum temperatures $T_{\rm max} = 50^{\circ}$ C, 100° C and 200° C are used to apply the thermal load with settling time at 0.5 s for total time duration of 1 s. Figure 5 shows the temperature profile when applied over a period of 2 s. The two-second temperature profiles are used for the slider crank mechanism example discussed later in this section.

In case of an unconstrained beam, the final thermal expansion of an isotropic material along an axis is proportional to the length along this axis and temperature change. In case of unconstrained planar ANCF shear-deformable beam element under effect of thermal load and without rotations, the displacement of the left and right endpoints are expected to be equal in magnitude and opposite in direction, and the stretch can be measured by the norm of the position gradient vectors \mathbf{r}_x and \mathbf{r}_y . The expansion in the beam cross section measured by the change of the norm of \mathbf{r}_{v} due to thermal load cannot be captured using conventional FE beam formulations that use rotations as nodal coordinates and ignore Poisson effect (Shabana and Zhang 2021; Eldeeb, Zhang, and Shabana 2022). Figure 6 shows that the axial deformation reaches the expected values for each temperature. The results of Fig. 6 are verified analytically using definition of the linear coefficient of thermal expansion and data of this example. For a 200°C temperature, the total elongation $\triangle l$ can be calculated as $\triangle l = \alpha l \triangle \theta = 0.0001 \times 1 \times 200 = 0.02$ m. For a uniform and free thermal expansion, each node is expected to move by 0.01 m, which is half the total elongation, as shown in Fig. 3, verifying the results presented in Fig. 6. Figures 7 and 8 show that the norms of the position vector

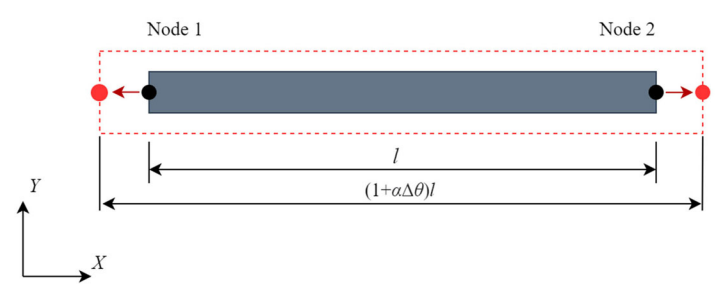


Figure 3. Unconstrained beam subjected to thermal load.

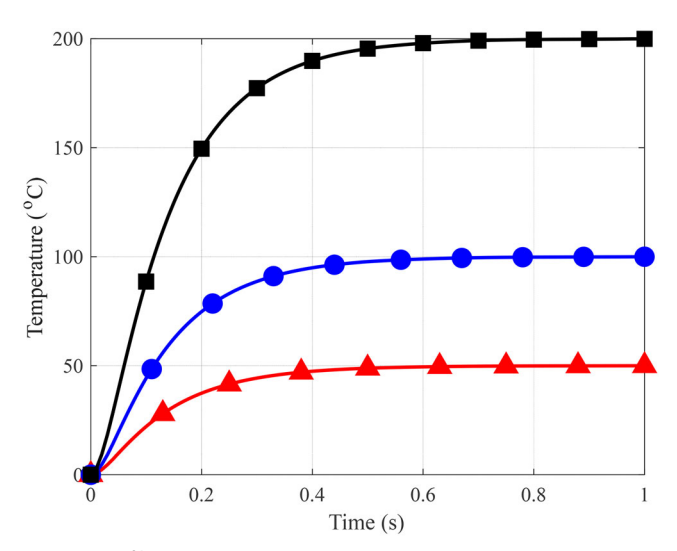


Figure 4. One-second temperature profile.

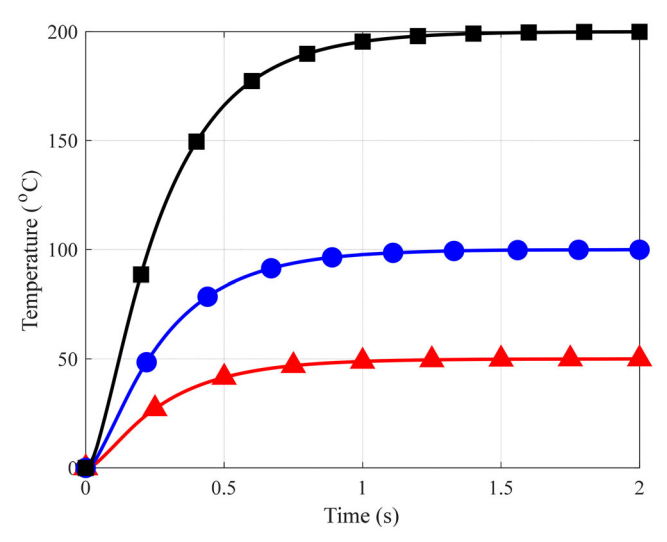


Figure 5. Two-second temperature profile.

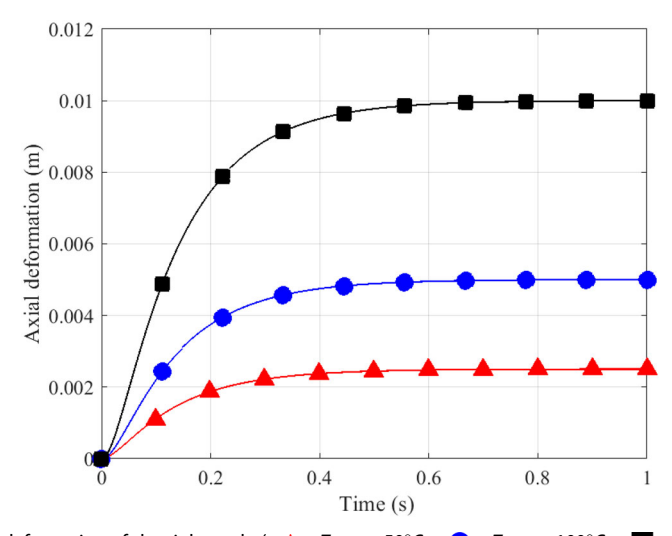


Figure 6. Axial thermal deformation of the right node ($-\triangle - T_{max} = 50^{\circ}\text{C}$, $-\bigcirc - T_{max} = 100^{\circ}\text{C}$, $-\boxed{\blacksquare} - T_{max} = 200^{\circ}\text{C}$).

gradients \mathbf{r}_x and \mathbf{r}_y increase to their expected values for the given temperature profile. Figure 9 shows a comparison between calculated nodal displacement using the ANCF approach described in this investigation and the analytical solution. This comparison shows a good agreement between the two solutions. The right node velocity is shown in Fig. 10 for different temperature profiles. It is shown that the node has an acceleration at the beginning of the simulation and the acceleration approaches zero as the temperature assumes constant value. Figure 11 shows the kinetic energy of the beam due the application of the thermal load. The results in this figure show that the kinetic energy has the expected profile of initial increase followed by decrease to the zero value. The analytical values of the nodal velocities and the mass matrix of the beam were used to calculate the kinetic energy analytically. Figure 12 shows the comparison between the numerical and analytical solutions of the kinetic energy at 200° C temperature.

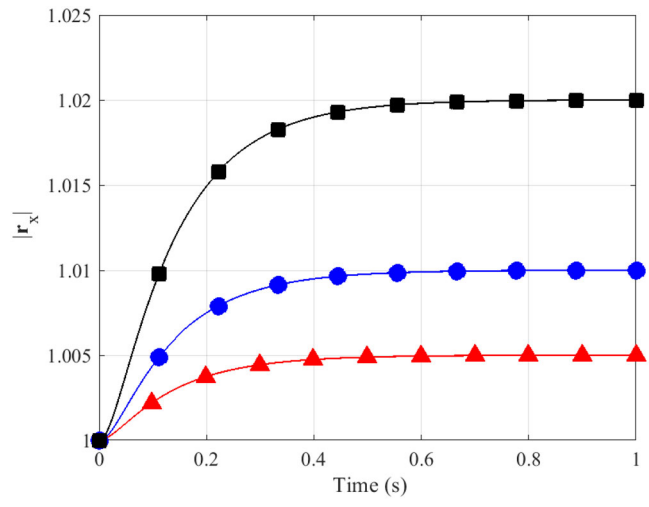


Figure 7. Norm of the position vector gradient \mathbf{r}_{x} ($-\mathbf{A} - T_{max} = 50^{\circ}$ C, $-\mathbf{C} - T_{max} = 100^{\circ}$ C, $-\mathbf{C} - T_{max} = 200^{\circ}$ C).

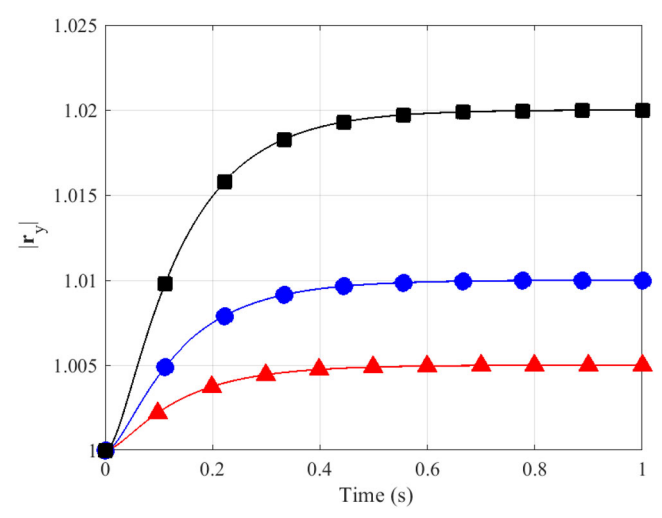


Figure 8. Norm of the position vector gradient \mathbf{r}_y ($-\Delta - T_{max} = 50^{\circ}$ C, $-\mathbf{T}_{max} = 100^{\circ}$ C, $-\mathbf{T}_{max} = 100^{\circ}$ C, $-\mathbf{T}_{max} = 200^{\circ}$ C).

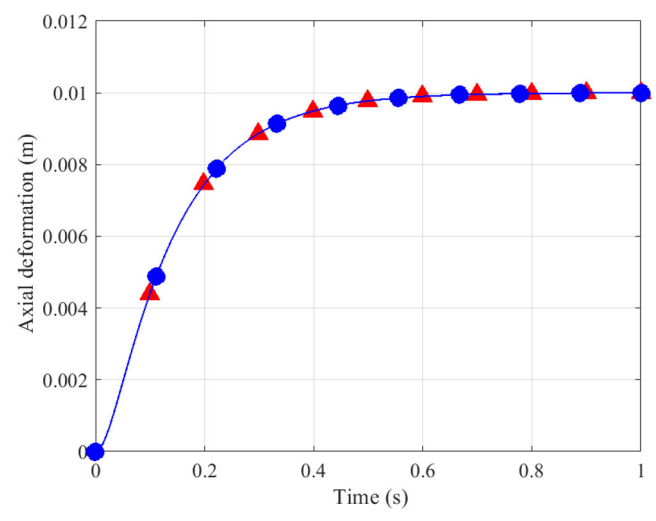


Figure 9. Axial thermal deformation of the right node at $T_{max} = 200^{\circ}\text{C}$ ($-\triangle$ —Analytical, $-\bigcirc$ —ANCF solution).

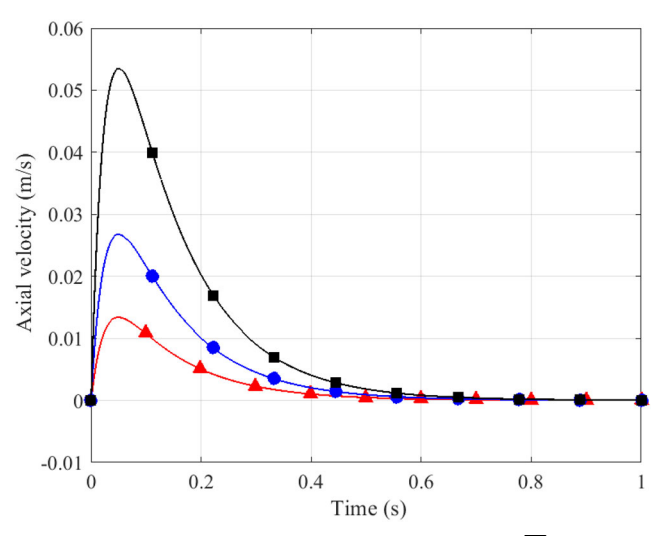


Figure 10. Axial velocity of the right node ($-\triangle - T_{max} = 50^{\circ}\text{C}$, $-\bigcirc - T_{max} = 100^{\circ}\text{C}$, $-\bigcirc - T_{max} = 200^{\circ}\text{C}$).

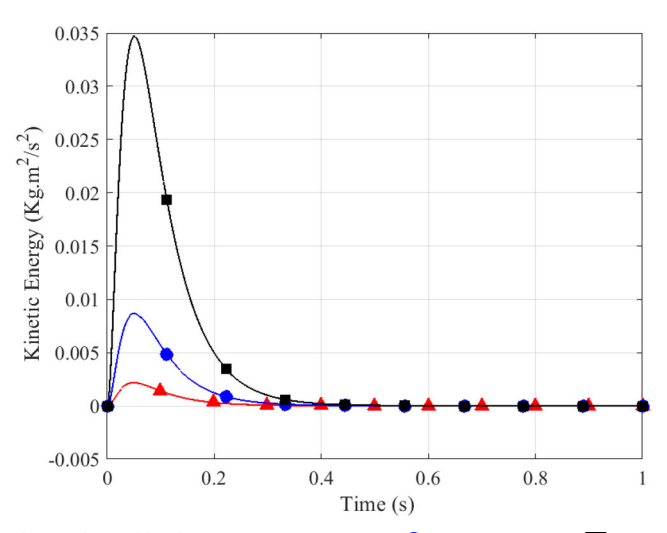


Figure 11. Kinetic energy due to thermal loading ($-\triangle - T_{max} = 50^{\circ}$ C, $-\bigcirc - T_{max} = 100^{\circ}$ C, $-\bigcirc - T_{max} = 100^{\circ}$ C).

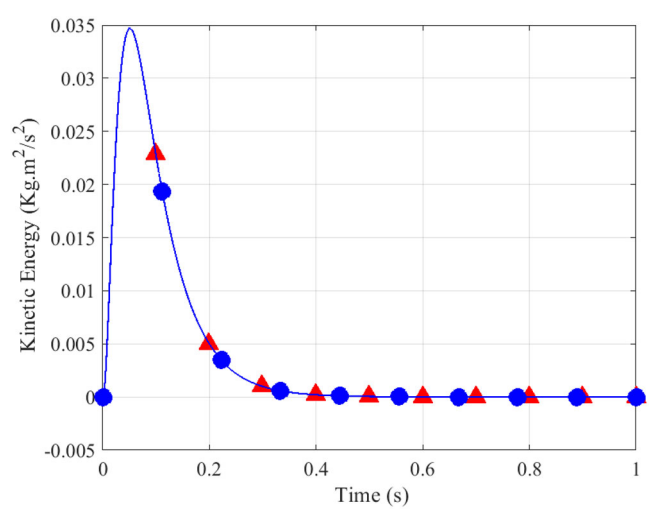


Figure 12. Kinetic energy for temperature profile $T_{max} = 200^{\circ}\text{C}$ ($-\triangle$ Analytical, $-\bigcirc$ ANCF solution).

11.2. Application to multibody system

In order to examine the effect of thermal expansion on the solution of MBS problems, the slider crank mechanism example shown in Fig. 13 is considered. The mechanism has four bodies: ground, crankshaft, connecting rod, and slider block. The crankshaft has length of 0.152 m while length of the connecting rod is $0.304\,\mathrm{m}$ with cross-sectional area $A = (5.5 \times 10^{-3}) \times (5.76 \times 10^{-3})$ 10⁻³) m². All bodies are assumed rigid except the flexible connecting rod, which is made of soft material with modulus of elasticity $E=2\times10^8$ Pa, Poisson ratio $\nu=0.3$, mass density $\rho=0.3$ 7200kg/m^3 , and coefficient of thermal expansion $\alpha = 80 \times 10^{-6} \ (1/^{\circ}\text{C})$. The connecting rod is modeled using six ANCF fully parameterized planar beam elements. The slider block is assumed massless, and the gravity effect is ignored for all the bodies. The crankshaft and the connecting rod are assumed initially horizontal. The crankshaft is assumed to rotate with constant angular velocity $\omega = \pi$ rad/s while the connecting rod is subjected to the thermal load. In this example, the temperature changes gradually, as shown in Fig. 5, reaching maximum values of $T_{\rm max} = 50^{\circ}$ C, 100° C, and 200° C. Figure 14 shows the transverse deformation of the mid-point of the connecting rod for different temperatures. Because the material properties are assumed constant and do not depend on temperature in this example, the results show that the maximum value of the deformation decreases as the temperature increases for this example. This decrease in the midpoint transverse deformation may not be interpreted as stiffening due to the increase in the dimensions. On the contrary, the increase in temperature leads to slight softening. To study the temperature effect on the stiffness, a simply supported beam of the same material with

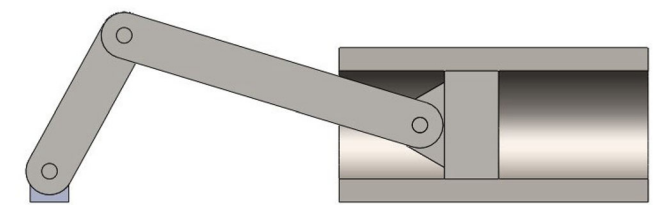


Figure 13. Slider crank mechanism.

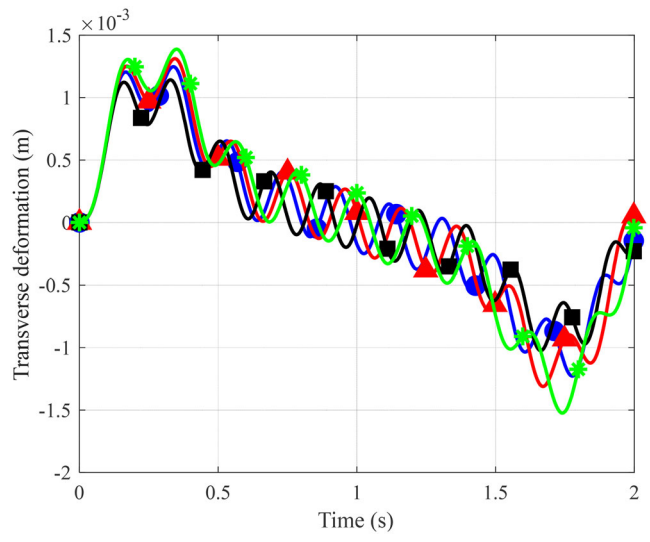


Figure 14. Mid-point transverse deformation at different thermal loads ($\underline{} * \underline{}$ No thermal load, $\underline{} * \underline{}$, $T_{max} = 50^{\circ}$ C, $\underline{} * \underline{} * \underline{}$ No thermal load, $\underline{} * \underline{} * \underline{$

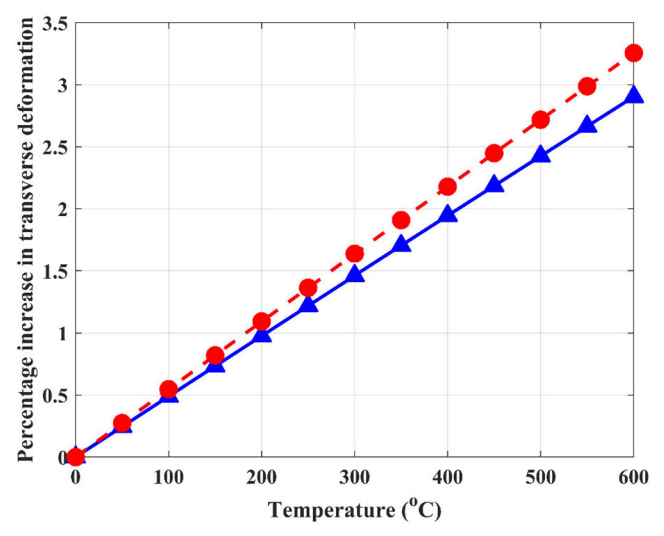


Figure 15. Percentage increase in static midpoint transverse deformation at different uniform thermal loads (- $F_{tr} = -3000 \text{ N}, \quad -F_{tr} = -6000 \text{ N}.$

dimensions $1 \times 0.05 \times 0.05$ m³ is considered. The beam is subjected to a midpoint transverse load F_{tr} and a uniform thermal load. Figure 15 shows the percentage increase in the midpoint static deflection for different values of the thermal loads. The results show that the stiffness remains almost constant. Preliminary results have shown that if the material properties are varied with temperature, the increase in temperature can have a softening effect. These results will be reported in a future investigation. Figure 16 shows the effect of the temperature profile on the dynamic response. The figure shows the mid-point transverse deformation in two scenarios at which the temperature reaches maximum value of 50°C. In the first scenario, the thermal load shown in Fig. 5 is applied, while in the second scenario the load is applied as a step input. In case of the step thermal load, initial compressive stresses are generated at the beginning of the simulation. These initial stresses excite higher frequencies and lead to increase in the deformation

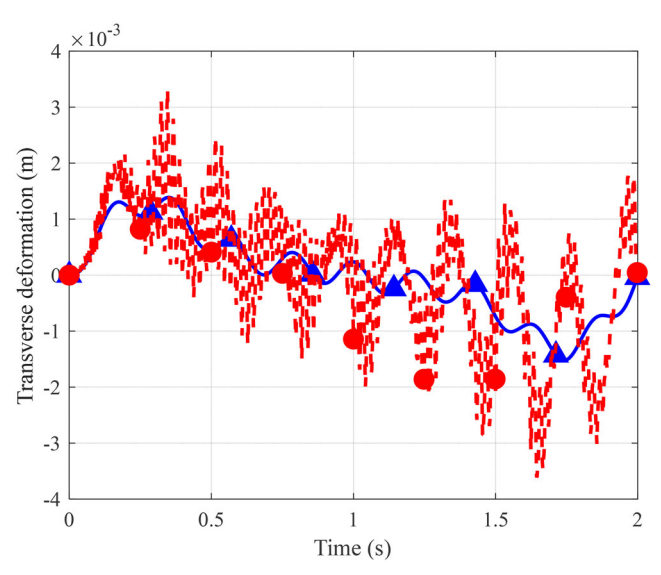


Figure 16. Effect of temperature profile on the dynamic response in case of maximum temperature $T_{max} = 50^{\circ}\text{C}$ (— Δ – Gradual rise, _ _ _ _ Step rise).

magnitude (Shabana, Elbakly, and Zhang 2023). In this case, the compressive forces due to the inertia are expected regardless of the method used to model the thermal expansion. However, this loading case was chosen as an example of extreme thermal loading rate. It is important to mention that the results obtained in this numerical study are based on the assumption that the thermal expansion is defined along the reference-configuration position-gradient vectors and not along current-configuration position-gradient vectors. This fundamental issue will be examined in future investigations since preliminary results obtained demonstrate differences between the two solutions that correspond to the two sets of position-gradients.

12. Summary and conclusions

Thermal expansion does not lead to rigid-body displacements and results in pure stretches with no distortion if no constraints are imposed on the continuum motion. If effects of heat dissipation to environment and cooling are not considered, the heat-energy converted to kinetic energy can be formulated in terms of the temperature derivatives and used to compute thermal-energy forces. Furthermore, in case of AMS applications, governed by Lagrange-D'Alembert principle, definition of thermal-expansion displacements is necessary for formulating inertia forces due to temperature change. To capture the dynamic effects of the thermo-elasticity problem and avoid using quasi-static approaches, new solution framework for thermal analysis of articulated systems (TAAS) subject to boundary and motion constraints (BMC) is proposed in this study. The proposed solution framework can capture large temperature fluctuations, significant change in geometry due to reference configuration and deformations, and geometric nonlinearity due to AMS large displacements and spinning motion. New sweeping matrix technique is used to eliminate dependence of the thermal displacements on translational rigid-body modes and eliminate singularity of coefficient matrices required in the formulation proposed in the paper. New quadratic thermal-energy form, referred to as thermal-energy kinetic form is introduced and used to formulate thermal-energy force vector that captures thermal transient and inertia effects. Thermal stresses due to BMC restrictions are accounted for by integrating thermal analysis and Lagrange-D'Alembert principle. The approach used in this study for large-displacement thermal analysis is based on multiplicative decomposition of position-gradient matrix, instead of strain additive decomposition. Four configurations are used to define continuum geometry and displacements: straight configuration, reference configuration, thermal-expansion configuration, and current configuration. Numerical results are presented to demonstrate the implementation and use of the approach introduced in the paper.

Funding

This research was supported by the National Science Foundation (Projects # 1852510).

Data availability statement

The data of the models developed in the paper are presented in the numerical example section.

Disclosure statement

The author declares that they have no conflict of interest.

References

Abbas, L. K., X. Rui, and P. Marzocca. 2015. Aerothermoelastic analysis of panel flutter based on the absolute nodal coordinate formulation. Multibody System Dynamics 33 (2):163-78. doi:10.1007/s11044-014-9410-2.



API Manual of Petroleum Measurement Standards (MPMS). 2004. Chapter 11.1-20041/Adjunct to ASTM D1250-04²/Adjunct to IP 200/04. Temperature and Pressure Volume Correction Factors for Generalized Crude Oils. Refined Products, and Lubricating Oils/Addendum 1-2007.

Biot, M. A. 1956. Thermoelasticity and irreversible thermodynamics. Journal of Applied Physics 27 (3):240-53. doi: 10.1063/1.1722351.

Bonet, J., and R. D. Wood. 1997. Nonlinear continuum mechanics for finite element analysis. New York, NY: Cambridge University Press.

Bower, A. F. 2009. Applied mechanics of solids. 1st ed. Boca Raton, FL: CRC Press.

Cepon, E., G. Starc, B. ZupančIč, B, and Boltežar, M. 2017. Coupled thermo-structural analysis of a bimetallic strip using the absolute nodal coordinate formulation. Multibody System Dynamics 41:391-402. doi:10.1007/s11044-017-9574-7.

Chen, Y., D. G. Zhang, and L. Li. 2019. Dynamic analysis of rotating curved beams by using absolute nodal coordinate formulation based on radial point interpolation method. Journal of Sound and Vibration 441:63-83. doi: 10.1016/j.jsv.2018.10.011.

Cook, R. D. 1981. Concepts and applications of finite element analysis. New York: Wiley.

Cui, Y., Z. Yu, and P. Lan. 2019. A novel method of thermo-mechanical coupled analysis based on the unified description. Mechanism and Machine Theory 134:376-92. doi:10.1016/j.mechmachtheory.2019.01.001.

Darijani, H. 2012. Finite deformation thermoelasticity of thick-walled cylindrical vessels based on the multiplicative decomposition of deformation gradient. Journal of Thermal Stresses 35 (12):1143-57. doi:10.1080/01495739.2012. 720531.

Darijani, H., and M. H. Kargarnovin. 2010. Kinematics and Kinetics description of thermoelastic finite deformation from multiplicative decomposition of deformation gradient viewpoint. Mechanics Research Communications 37 (6):515-9. doi:10.1016/j.mechrescom.2010.07.013.

Darijani, H., and R. Naghdabadi. 2013. Kinematics and kinetics modeling of thermoelastic continua based on the multiplicative decomposition of the deformation gradient. International Journal of Engineering Science 73:77. doi:10.1016/j.ijengsci.2013.09.002.

Dmitrochenko, O. N., and D. Y. Pogorelov. 2003. Generalization of plate finite elements for absolute nodal coordinate formulation. Multibody System Dynamics 10 (1):17-43. doi:10.1023/A:1024553708730.

Dorfman, A., and Z. Renner. 2009. Conjugate problems in convective heat transfer: Review. Mathematical Problems in Engineering 2009:1-27. doi:10.1155/2009/927350.

Dwaikat, M. M. S., and Kodur, V. K. R. 2011. A performance based methodology for fire design of restrained steel beams. Journal of Constructional Steel Research 67 (3):510-24. doi:10.1016/j.jcsr.2010.09.004.

Eckart, C. 1948. The thermodynamics of irreversible processes. IV. The theory of elasticity and anelasticity. Physical Review 73 (4):373-82. doi:10.1103/PhysRev.73.373.

Eldeeb, A. E., D. Zhang, and A. A. Shabana. 2022. Cross-section deformation, geometric stiffening, and locking in the nonlinear vibration analysis of beams. Nonlinear Dynamics 108:1425-45.

Engineering ToolBox. 2003. Coefficients of linear thermal expansion. https://www.engineeringtoolbox.com/linearexpansion-coefficients-d_95.html.

Errera, M.-P., and S. Chemin. 2013. Optimal solutions of numerical interface conditions in fluid-structure thermal analysis. Journal of Computational Physics 245:431-55. doi:10.1016/j.jcp.2013.03.004.

Eslami, M. R., R. B. Hetnarski, J. Ignaczak, N. Noda, N. Sumi, and Y. Tanigawa. 2013. Theory of elasticity and thermal stresses. New York: Springer.

Farin, G. 2002. Curves and surfaces for CAGD, a practical guide. 5th ed. San Francisco: Morgan Kaufmann.

Fotland, G., C. Haskins, and T. Rølvåg. 2019. Trade study to select best alternative for cable and pulley simulation for cranes on offshore vessels. Systems Engineering 23 (2):177-88. doi:10.1002/sys.21503.

Gallier, J. 2011. Geometric methods and applications: For computer science and engineering. New York: Springer.

Gerstmayr, J., and A. A. Shabana. 2005. Efficient integration of the elastic forces and thin threedimensional beam elements in the absolute nodal coordinate formulation. Multibody Dynamics 2005, ECCOMAS Thematic conference, Madrid, Spain.

Goetz, A. 1970. Introduction to differential geometry. Boston, MA: Addison Wesley.

Heidarpour, A., and M. A. Bradford. 2009. Generic nonlinear modelling of restrained steel beams at elevated temperatures. Engineering Structures 31 (11):2787-96. doi:10.1016/j.engstruct.2009.07.006.

Helselhaus, A., T. Vogel, and H. Krain. 1992. Coupling of 3D-Navier-Stokes external flow calculations and internal 3D-heat conduction calculations for cooled turbine blades. Proceedings of the AGARD Meeting on Heat Transfer and Cooling in Gas Turbines, AGARD-CP-527, 40-1-40-9.

Henshaw, W. D., and K. K. Chand. 2009. A composite grid solver for conjugate heat transfer in fluid-structure systems. Journal of Computational Physics 228 (10):3708-41. doi:10.1016/j.jcp.2009.02.007.

Hewlett, J. 2019. Methods for real-time simulation of systems of rigid and flexible bodies with unilateral contact and friction. Ph.D. Thesis, Department of Mechanical Engineering, McGill University.



- Hewlett, J., S. Arbatani, and J. Kovecses. 2020. A fast and stable first-order method for simulation of flexible beams and cables. Nonlinear Dynamics 99 (2):1211-26. doi:10.1007/s11071-019-05347-1.
- Htun, T. Z., H. Suzuki, and D. Garcia-Vallejo. 2020. Dynamic modeling of a radially multilayered tether cable for a remotely-operated underwater vehicle (ROV). Based on the absolute nodal coordinate formulation (ANCF). Mechanism and Machine Theory 153:103961. doi:10.1016/j.mechmachtheory.2020.103961.
- Huang, X., J. Zou, and G. Gu. 2021. Kinematic modeling and control of variable curvature soft continuum robots. IEEE/ASME Transactions on Mechatronics 26 (6):3175-85. doi:10.1109/TMECH.2021.3055339.
- Huang, Z., and K. Tan. 2004. Effects of external bending moments and heating schemes on the responses of thermally restrained steel columns. Engineering Structures 26 (6):769-80. doi:10.1016/j.engstruct.2004.01.010.
- Imam, A., and G. C. Johnson. 1998. Decomposition of deformation gradient in thermoelasticity. Journal of Applied Mechanics 65 (2):362-6. doi:10.1115/1.2789063.
- Joulin, C., J. S. Xiang, and J. P. Latham. 2020. A novel thermo-mechanical coupling approach for thermal fracturing of rocks in the three-dimensional FDEM. Computational Particle Mechanics 7 (5):935-46. doi:10.1007/ s40571-020-00319-4.
- Khan, I. M., and K. S. Anderson. 2013. Divide-and-conquer-based large deformation formulations for multi-flexible body systems. Proceedings of the ASME 9th International Conference on Multibody Systems, Nonlinear Dynamics, and Control, Vol. 7B, Portland, Oregon, USA, V07BT10A002-1-10.
- Kreyszig, E. 1991. Differential geometry. New York, NY: Dover Publications.
- Kroner, E. 1959. Allgemeine Kontinuumstheorie der Versetzungen und Eigensspannungen. Archive for Rational Mechanics and Analysis 4 (1):273-334. doi:10.1007/BF00281393.
- Laflin, J. J., K. S. Anderson, I. M. Khan, and M. Poursina. 2014. New and extended applications of the divide-andconquer algorithm for multibody dynamics. ASME Journal of Computational and Nonlinear Dynamics 9 (4):
- Li, S., Y. Wang, X. Ma, and S. Wang. 2019. Modeling and simulation of a moving yarn segment: Based on the absolute nodal coordinate formulation. Mathematical Problems in Engineering 2019:6567802. doi:10.1155/2019/ 6567802.
- Li, Y., C. Wang, and W. Huang. 2019. Rigid-flexible-thermal analysis of planar composite solar array with clearance joint considering torsional spring, latch mechanism and attitude controller. Nonlinear Dynamics 96 (3): 2031-53. doi:10.1007/s11071-019-04903-z.
- Liu, J. Y., and H. Lu. 2007. Thermal effect on the deformation of a flexible beam with large kinematical driven overall motion. European Journal of Mechanics 26 (1):137-51. doi:10.1016/j.euromechsol.2006.04.001.
- Logan, D. L. 2017. A first course in the finite element method. 6th ed., Chap. 15. Cengage Learning.
- Longère, P., A. Dragon, H. Trumel, and X. Deprince. 2005. Adiabatic shear banding-induced degradation in a thermo-elastic/viscoplastic material under dynamic loading. International Journal of Impact Engineering 32 (1-4):285-320. doi:10.1016/j.ijimpeng.2005.03.002.
- Lubarda, V. A. 2004. Constitutive theories based on the multiplicative decomposition of deformation gradient: Thermoelasticity, elastoplasticity, and biomechanics. Applied Mechanics Reviews 57 (2):95-108. doi:10.1115/1.
- Manolis, G. D., and D. E. Beskos. 1980. Thermally induced vibrations of beam structures. Computer Methods in Applied Mechanics and Engineering 21 (3):337-55. doi:10.1016/0045-7825(80)90101-2.
- Miehe, C. 1995. Entropic thermoelasticity at finite strains, aspects of the formulation and numerical implementation. Computer Methods in Applied Mechanics and Engineering 120 (3-4):243-69. doi:10.1016/0045-7825(94)00057-T.
- Nachbagauer, K. 2013. Development of shear and cross section deformable beam finite elements applied to large deformation and dynamics problems. Ph.D. dissertation, Johannes Kepler University, Linz, Austria.
- Nachbagauer, K. 2014. State of the art of ANCF elements regarding geometric description, interpolation strategies, definition of elastic forces, validation and locking phenomenon in comparison with proposed beam finite elements. Archives of Computational Methods in Engineering 21 (3):293-319. doi:10.1007/s11831-014-9117-9.
- Nachbagauer, K., A. S. Pechstein, H. Irschik, and J. Gerstmayr. 2011. A new locking-free formulation for planar, shear deformable, linear and quadratic beam finite elements based on the absolute nodal coordinate formulation. Multibody System Dynamics 26 (3):245-63. doi:10.1007/s11044-011-9249-8.
- Ogden, R. W. 1984. Non-linear elastic deformations. Mineola, NY: Dovers Publications.
- Ojas, J., and L. Penelope. 2014. Stability analysis of a partitioned fluid-structure thermal coupling algorithm. Journal of Thermophysics and Heat Transfer 28 (1):59-67. doi:10.2514/1.T4032.
- Olshevskiy, A., O. Dmitrochenko, and C. W. Kim. 2014. Three-dimensional solid brick element using slopes in the absolute nodal coordinate formulation. ASME Journal of Computational and Nonlinear Dynamics 9 (2):021001-1-10.
- Omar, M. A., A. Shabana, A. Mikkola, W.-Y. Loh, and R. Basch. 2004. Multibody system modeling of leaf springs. Journal of Vibration and Control 10 (11):1601-38. doi:10.1177/1077546304042047.



Orzechowski, G. 2012. Analysis of beam elements of circular cross section using the absolute nodal coordinate formulation. Archive of Mechanical Engineering 59 (3):283-96. doi:10.2478/v10180-012-0014-1.

Orzechowski, G., and J. Fraczek. 2012. Integration of the equations of motion of multibody systems using absolute nodal coordinate formulation. Acta Mechanica et Automatica 6 (2):75-83.

Pan, K., and D. Cao. 2020. Absolute nodal coordinate finite element approach to the two-dimensional liquid sloshing problems. Proceedings of the Institution of Mechanical Engineers, Part K: Journal of Multi-Body Dynamics 234(2), 1–25. doi:10.1177/1464419320907785.

Pappalardo, C. M., M. Wallin, and A. A. Shabana. 2016. A new ANCF/CRBF fully parameterized plate finite element. ASME Journal of Computational and Nonlinear Dynamics 12 (3):031008. doi:10.1115/1.4034492.

Pappalardo, C. M., Z. Yu, X. Zhang, and A. A. Shabana. 2016. Rational ANCF thin plate finite element. ASME Journal of Computational and Nonlinear Dynamics 11 (5):051009. doi:10.1115/1.4032385.

Perelman, T. L. 1961. On conjugated problems of heat transfer. International Journal of Heat and Mass Transfer 3 (4):293-303. doi:10.1016/0017-9310(61)90044-8.

Piegl, L., and W. Tiller. 1997. The NURBS book. 2nd ed. Berlin: Springer.

Pournaghshband, A., S. Afshan, and M. Theofanous. 2019. Elevated temperature performance of restrained stainless steel beams. Structures 22:278-90. doi:10.1016/j.istruc.2019.08.015.

Roe, B., A. Haselbacher, and P. H. Geubelle. 2007. Stability of fluid-structure thermal simulations on moving grids. International Journal for Numerical Methods in Fluids 54 (9):1097-117. doi:10.1002/fld.1416.

Roe, B., R. Jaiman, A. Haselbacher, and P. H. Geubelle. 2008. Combined interface boundary method for coupled thermal simulations. International Journal for Numerical Methods in Fluids 57 (3):329-54. doi:10.1002/fld.1637.

Rogers, D. F. 2001. An introduction to NURBS with historical perspective. San Diego, CA: Academic Press.

Rus, D., and M. T. Tolley. 2015. Design, fabrication and control of soft robots. Nature 521 (7553):467-75. doi:10. 1038/nature14543.

Sadik, S., and A. Yavari. 2017. On the origins of the idea of the multiplicative decomposition of the deformation gradient. Mathematics and Mechanics of Solids 22 (4):771-2. doi:10.1177/1081286515612280.

Sauer, R. A., R. Ghaffari, and A. Gupta. 2019. The multiplicative deformation split for shells with application to growth, chemical swelling, thermoelasticity, viscoelasticity and elastoplasticity. International Journal of Solids and Structures 174-175:53-68. doi:10.1016/j.ijsolstr.2019.06.002.

Sedov, L. 1966. Foundations of the non-linear mechanics of continua. Oxford: Pergamon Press.

Seibert, A. G., and J. S. Rice. 1973. Coupled thermally induced vibrations of beams. AIAA Journal 11 (7):1033-5. doi:10.2514/3.6866.

Shabana, A. A. 1986. Thermal analysis of viscoelastic multibody systems. Mechanism and Machine Theory 21 (3): 231-42. doi:10.1016/0094-114X(86)90099-6.

Shabana, A. A. 2015. Definition of ANCF finite elements. ASME Journal of Computational and Nonlinear Dynamics 10:054506-1-5.

Shabana, A. A. 2018. Computational continuum mechanics. 3rd ed. Cambridge: Cambridge University Press.

Shabana, A. A. 2019. Vibration of discrete and continuous systems. 3rd ed. New York: Springer.

Shabana, A. A., M. Elbakly, and D. Zhang. 2023. Constrained large-displacement thermal analysis. Journal of Computational and Nonlinear Dynamics 18 (2):021002-13. doi:10.1115/1.4056182

Shabana, A. A., and D. Zhang. 2021. ANCF multiplicative-decomposition thermo-elastic approach for arbitrary geometry. Journal of Structural Engineering 147 (7):04021086-1-11. doi:10.1061/(ASCE)ST.1943-541X.0003001.

Shen, Z., and G. Hu. 2013. Thermally induced vibrations of solar panel and their coupling with satellite. International Journal of Applied Mechanics 55 (3):1350031.

Shen, Z., C. Liu, and H. Li. 2020. Viscoelastic analysis of bistable composite shells via absolute nodal coordinate formulation. Composite Structures 248:112537. doi:10.1016/j.compstruct.

Shen, Z., Q. Tian, X. Liu, and G. Hu. 2013. Thermally induced vibrations of flexible beams using absolute nodal coordinate formulation. Aerospace Science and Technology 29 (1):386-93. doi:10.1016/j.ast.2013.04.009.

Sheng, F., Z. Zhong, and K. Wang. 2020. Theory and model implementation for analyzing line structures subject to dynamic motions of large deformation and elongation using the absolute nodal coordinate formulation (ANCF) approach. Nonlinear Dynamics 101 (1):333-59. doi:10.1007/s11071-020-05783-4.

Spencer, A. J. M. 1980. Continuum mechanics. London: Longman.

Stojanovic, R. 1969. On the stress relation in non-linear thermoelasticity. International Journal of Non-Linear Mechanics 4:217-33.

Stojanovic, R., S. Djuric, and L. Vujosevic. 1964. On finite thermal deformations. Archiwum Mechaniki Stosowanej

Stojanovic, R., L. Vujosevic, and D. Blagojevic. 1970. Couple stresses in thermoelasticity. Revue Roumaine Des Sciences Techniques - Série de Mécanique Appliquée 15:517-37.

Takahashi, Y., N. Shimizu, and K. Suzuki. 2005. Study on the frame structure modeling of the beam element formulated by absolute coordinate approach. Journal of Mechanical Science and Technology 19 (S1):283-291. doi: 10.1007/BF02916146.



- Thomson, W. T. 1993. Theory of vibration with applications. 4th ed. Englewood Cliffs, NJ: Prentice Hall.
- Tian, Q., L. Chen, Y. Zhang, and J. Yang. 2009. An efficient hybrid method for multibody dynamics simulation based on absolute nodal coordinate formulation. ASME Journal of Computational and Nonlinear Dynamics 4 (2):021009-1-14.
- Trivedi, D., D. Dienno, and C. D. Rahn. 2008. Optimal, model-based design of soft robotic manipulators. Journal of Mechanical Design 130 (9):091402-1-9. doi:10.1115/1.2943300.
- Vujosevic, L., and V. A. Lubarda. 2002. Finite-strain thermoelasticity based on multiplicative decomposition of deformation gradient. Theoretical and Applied Mechanics 28-29:379-99.
- Wang, J., and T. Wang. 2020. Buckling analysis of beam structure with absolute nodal coordinate formulation. IMechE Journal of Mechanical Engineering Science 235 (9):1585-8. doi:10.1177/0954406220947117.
- Weaver, W., S. P. Timoshenko, and D. H. Young. 1990. Vibration problems in engineering. 5th ed. New York: Wiley & Sons.
- Wu, J., Z. H. Zhao, and G. X. Ren. 2012. Dynamic analysis of space structure deployment with transient thermal load. Advanced Materials Research 479-481:803-7. doi:10.4028/www.scientific.net/AMR.479-481.803.
- Yamano, A., A. Shintani, T. Ito, C. Nakagawa, and H. Ijima. 2020. Influence of boundary conditions on a fluttermill. Journal of Sound and Vibration 478:115359. doi:10.1016/j.jsv.2020.115359.
- Yin, Y. Z., and Y. C. Wang. 2004. A numerical study of large deflection behaviour of restrained steel beams at elevated temperatures. Journal of Constructional Steel Research 60 (7):1029-47. doi:10.1016/j.jcsr.2003.09.005.
- Yoo, W.-S., J.-H. Lee, S.-J. Park, J.-H. Sohn, D. Pogorelov, and O. Dmitrochenko. 2004. Large deflection analysis of a thin plate: Computer simulation and experiment. Multibody System Dynamics 11 (2):185-208. doi:10.1023/ B:MUBO.0000025415.73019.bb.
- Yu, L., Z. Zhao, J. Tang, and G. Ren. 2010. Integration of absolute nodal elements into multibody system. Nonlinear Dynamics 62 (4):931-943. doi:10.1007/s11071-010-9775-6.
- Yuan, T., Z. Liu, Y. Zhou, and J. Liu. 2020. Dynamic modeling for foldable origami space membrane structure with contact-impact during deployment. Multibody System Dynamics 50 (1):1-24. doi:10.1007/s11044-020-
- Zhang, W., W. Zhu, and S. Zhang. 2020. Deployment dynamics for a flexible solar array composed of compositelaminated plates. Journal of Aerospace Engineering 33 (6):04020071-1-21. doi:10.1061/(ASCE)AS.1943-5525.
- Zienkiewicz, O. C. 1977. The finite element method. 3rd ed. New York: McGraw Hill.
- Zienkiewicz, O. C., and Taylor, R. L. 2000. The finite element method, Vol. 2: Solid Mechanics. Vol. 5. Oxford: Butterworth-Heinemann.



Appendix

In this appendix, the planar shear-deformable fully parameterized ANCF beam element is used as an example to provide explicit forms of some matrices required for the implementation of the formulation proposed in this paper. The planar ANCF beam element has two nodes; and each node k has six nodal coordinates, two position coordinates and four position-gradient coordinates. The element displacement field can be written as $\mathbf{r}(\mathbf{x},t)$ S(x)e(t). Vector of element nodal coordinate e and shape-function matrix S can be written, respectively, as

$$\mathbf{e}(t) = \begin{bmatrix} e_1 \ e_2 \cdots e_{12} \end{bmatrix}^T = \begin{bmatrix} \mathbf{r}^{1^T} \ \mathbf{r}_{x_1}^{1^T} \ \mathbf{r}_{x_2}^{1^T} \ \mathbf{r}^{2^T} \ \mathbf{r}_{x_1}^{2^T} \ \mathbf{r}_{x_2}^{2^T} \end{bmatrix}^T,$$

$$\mathbf{S}(\mathbf{x}) = \begin{bmatrix} s_1 \mathbf{I} \ s_2 \mathbf{I} \ s_3 \mathbf{I} \ s_4 \mathbf{I} \ s_5 \mathbf{I} \ s_6 \mathbf{I} \end{bmatrix}$$
(A.1)

where superscript k, k = 1, 2, refers to node number, \mathbf{r}^k is nodal position, $\mathbf{r}_{x_l} = \partial \mathbf{r} / \partial x_l$, l = 1, 2, are position-gradient vectors, and shape functions s_i , j = 1, 2, ..., 6, are defined as

$$\left. \begin{array}{l}
s_1 = 1 - 3\xi^2 + 2\xi^3, \, s_2 = l(\xi - 2\xi^2 + \xi^3), \, s_3 = l\eta(1 - \xi) \\
s_4 = 3\xi^2 - 2\xi^3, \, s_5 = l(-\xi^2 + \xi^3), \, s_6 = l\xi\eta \end{array} \right\} \tag{A.2}$$

In which $\xi = x_1/l$ and $\eta = x_2/l$. The mass matrix of the element is defined

$$\mathbf{M} = \int_{V} \rho \mathbf{S}^{T} \mathbf{S} dV$$

$$= m \begin{bmatrix} (13/35)\mathbf{I} & (11l/210)\mathbf{I} & \mathbf{0} & (9/70)\mathbf{I} & -(13l/420)\mathbf{I} & \mathbf{0} \\ (l^{2}/105)\mathbf{I} & \mathbf{0} & (13l/420)\mathbf{I} & -(l^{2}/140)\mathbf{I} & \mathbf{0} \\ & & (h^{2}/36)\mathbf{I} & \mathbf{0} & \mathbf{0} & (h^{2}/72)\mathbf{I} \\ & & & & (13/35)\mathbf{I} & -(11l/210)\mathbf{I} & \mathbf{0} \\ & & & & & (h^{2}/36)\mathbf{I} \end{bmatrix}$$
(A.3)
$$(A.3)$$

$$\text{Symm.} \qquad (l^{2}/105)\mathbf{I} \qquad \mathbf{0}$$

$$(h^{2}/36)\mathbf{I}$$

The integral of the element shape function is defined as

$$\bar{\mathbf{S}} = \int_{V} \rho \mathbf{S} \, dV = (m/2) \left[\mathbf{I} \, (l/6) \mathbf{I} \, \mathbf{0} \, \mathbf{I} \, - (l/6) \mathbf{I} \, \mathbf{0} \right]$$
 (A.4)

The inverse of the element mass matrix is

$$\mathbf{M}^{-1} = \left(\frac{4}{m}\right) \begin{bmatrix} 4\mathbf{I} - (30/l)\mathbf{I} & \mathbf{0} & -\mathbf{I} & -(15/l)\mathbf{I} & \mathbf{0} \\ (300/l^{2})\mathbf{I} & \mathbf{0} & (15/l)\mathbf{I} & (210/l^{2})\mathbf{I} & \mathbf{0} \\ (12/h^{2})\mathbf{I} & \mathbf{0} & \mathbf{0} & -(6/h^{2})\mathbf{I} \\ & 4\mathbf{I} & (30/l)\mathbf{I} & \mathbf{0} \\ & \text{Symm.} & (300/l^{2})\mathbf{I} & \mathbf{0} \\ & & & & & & & & & & & & & & & & \\ \end{bmatrix}$$
(A.5)

Using the fact that $s_1 - 1 = -3\xi^2 + 2\xi^3 = -s_4$, one can show that matrix \mathbf{S}_{rd} can be written as

$$\mathbf{S}_{rd} = \begin{bmatrix} -s_4 \mathbf{I} \ s_2 \mathbf{I} \ s_3 \mathbf{I} \ s_4 \mathbf{I} \ s_5 \mathbf{I} \ s_6 \mathbf{I} \end{bmatrix}$$
(A.6)

Using this matrix, matrix $\bar{\mathbf{M}}_{rd}$ can be evaluated as

$$\bar{\mathbf{M}}_{rd} = \int_{V} \rho \mathbf{S}_{rd}^{T} \mathbf{S}_{rd} dV$$

$$= m \begin{bmatrix} (13/35)\mathbf{I} & -(13l/420)\mathbf{I} & \mathbf{0} & -(13/35)\mathbf{I} & (11l/210)\mathbf{I} & \mathbf{0} \\ (l^{2}/105)\mathbf{I} & \mathbf{0} & (13l/420)\mathbf{I} & -(l^{2}/140)\mathbf{I} & \mathbf{0} \\ & & (h^{2}/36)\mathbf{I} & \mathbf{0} & \mathbf{0} & (h^{2}/72)\mathbf{I} \\ & & & & (13/35)\mathbf{I} & -(11l/210)\mathbf{I} & \mathbf{0} \\ & & & & & (l^{2}/105)\mathbf{I} & \mathbf{0} \\ & & & & & & (h^{2}/36)\mathbf{I} \end{bmatrix}$$
(A.7)

For one-element mesh, rigid-body translational modes A_{r_k} , k = 1, 2, can be defined as

$$\mathbf{A}_{r_k} = \begin{bmatrix} \mathbf{a}_{r_k}^T \ \mathbf{0}^T \ \mathbf{0}^T \ \mathbf{a}_{r_k}^T \ \mathbf{0}^T \ \mathbf{0}^T \end{bmatrix}^T, \quad k = 1, 2$$

$$\begin{bmatrix} \mathbf{a}_{r_1} \ \mathbf{a}_{r_2} \end{bmatrix} = \begin{bmatrix} 1 & 0 \\ 0 & 1 \end{bmatrix}, \quad \mathbf{0} = \begin{bmatrix} 0 \\ 0 \end{bmatrix}$$
(A.8)

Using translation rigid-body modes A_{r_k} , k = 1, 2, and element matrix M_{rd} , it can be shown that

$$\mathbf{S}\mathbf{A}_{r_k} = \mathbf{a}_{r_k}, \quad \mathbf{S}_{rd}\mathbf{A}_{r_k} = \mathbf{0}, \\
\mathbf{M}_{rd}\mathbf{A}_{r_k} = \mathbf{0}, \quad k = 1, 2$$
(A.9)

Furthermore, using two translational rigid-body modes, it can be shown that

$$\begin{bmatrix} \mathbf{A}_{r1} \ \mathbf{A}_{r2} \end{bmatrix}^T \mathbf{M} = m \begin{bmatrix} \mathbf{I}/2 \ \mathbf{I}l/12 \ \mathbf{0} \ \mathbf{I}/2 - \mathbf{I}l/12 \ \mathbf{0} \end{bmatrix}$$
(A.10)

One can also show that $\partial \mathbf{S}_{rd}/\partial x_l = \partial \mathbf{S}/\partial x_l$, l=1,2; that is, both \mathbf{S} and \mathbf{S}_{rd} lead to the same gradient vectors. This fact can be demonstrated by using shape function derivatives defined as

$$\begin{cases}
s_{1,1} = (6/l)(-\xi + \xi^2), & s_{2,1} = (1 - 4\xi + 3\xi^2), & s_{3,1} = -\eta, \\
s_{4,1} = (6/l)(\xi - \xi^2), & s_{5,1} = (-2\xi + 3\xi^2), & s_{6,1} = \eta, \\
s_{3,2} = (1 - \xi), & s_{6,2} = \xi
\end{cases}$$
(A.11)

Using conditions $\mathbf{A}_{r_k}^T \mathbf{M} \mathbf{e}_{d\Theta} = 0$, k = 1, 2, required to eliminate contribution of thermal expansion to translational rigid-body motion, one obtains coordinate transformation matrix \mathbf{H}_{di} as

$$\mathbf{H}_{di} = \begin{bmatrix} -(l/6)\mathbf{I} & \mathbf{0} & -\mathbf{I} & (l/6)\mathbf{I} & \mathbf{0} \\ \mathbf{I} & \mathbf{0} & \mathbf{0} & \mathbf{0} & \mathbf{0} \\ \mathbf{0} & \mathbf{I} & \mathbf{0} & \mathbf{0} & \mathbf{0} \\ \mathbf{0} & \mathbf{0} & \mathbf{I} & \mathbf{0} & \mathbf{0} \\ \mathbf{0} & \mathbf{0} & \mathbf{0} & \mathbf{I} & \mathbf{0} \\ \mathbf{0} & \mathbf{0} & \mathbf{0} & \mathbf{0} & \mathbf{I} \end{bmatrix}$$
(A.12)

This coordinate transformation shows that displacements of two element nodes as result of uniform thermal expansion are equal in magnitude and opposite in direction. It is also clear that

$$\mathbf{S}_{rd} \ \mathbf{H}_{di} = \left[s_2 \mathbf{I} \ s_3 \mathbf{I} \ 2s_4 \mathbf{I} \ s_5 \mathbf{I} \ s_6 \mathbf{I} \right] \tag{A.13}$$

This equation shows that matrix $\mathbf{M}_H = \mathbf{H}_{di}^T \mathbf{M}_{rd} \mathbf{H}_{di}$ is defined for this element as

$$\mathbf{M}_{H} = \mathbf{H}_{di}^{T} \mathbf{M}_{rd} \mathbf{H}_{di} = m \begin{bmatrix} (l^{2}/105)\mathbf{I} & \mathbf{0} & (13l/210)\mathbf{I} & (-l^{2}/140)\mathbf{I} & \mathbf{0} \\ & (h/6)^{2}\mathbf{I} & \mathbf{0} & \mathbf{0} & (h^{2}/72)\mathbf{I} \\ & & (52/35)\mathbf{I} & (-11l/105)\mathbf{I} & \mathbf{0} \\ & & & & (l^{2}/105)\mathbf{I} & \mathbf{0} \\ & & & & & & (h/6)^{2}\mathbf{I} \end{bmatrix}$$
(A.14)